

CZECH TECHNICAL UNIVERSITY IN PRAGUE
Faculty of Nuclear Sciences and Physical Engineering
Department of Physics

DEVELOPMENT OF POSITRON TRANSPORT AND
INJECTION FOR THE AEGIS EXPERIMENT

Diploma Thesis

submitted by

Daniel Krasnický

Supervisor: doc. RNDr. Vojtěch Petráček, CSc.

Prague 2009

Abstract

Název práce:

Vývoj transportu a injekce positronů v rámci experimentu AEGIS

Autor: Bc. Daniel Krasnický

Obor: Jaderné inženýrství

Druh práce: Diplomová práce

Vedoucí práce: doc. RNDr. Vojtěch Petráček, CSc. Katedra fyziky, Fakulta jaderná a fyzikálně inženýrská, České vysoké učení technické v Praze

Abstrakt: Experiment AEGIS bude produkovat chladný antivodík a provede první přímé měření působení gravitace na antimotlu. Cílem této práce bylo provedení simulací pohybu positronů v magnetickém poli experimentu AEGIS a následný návrh způsobu injekce positronů do hlavní části experimentu. Výsledkem práce je návrh positronové transfer linky, která pomocí cívek vede positrony z positronového akumulátoru do hlavního supravodivého magnetu. Positrony jsou radiálně udržovány a zároveň vedeny podélným magnetickým polem tvořeným hlavními cívkami obklopujícími vakuovou komoru. Pro korekci drah positronů jsou kolem hlavních vodících cívek navrženy páry Helmholtzových cívek. Součástí práce je souhrnný popis experimentu AEGIS, včetně metod chlazení antiprotonů a způsobu provedení gravitačního měření.

Klíčová slova: antivodík, AEGIS, chlazení antičástic, transfer positronů, gravitační měření.

Title:

Development of Positron Transfer and injection for the AEGIS experiment

Author: Daniel Krasnický

Abstract: AEGIS experiment will produce cold antihydrogen and subsequently make the first direct measurement of the gravitational effect on antimatter. The objective of this work was to perform simulations of positron motion in the magnetic field of the AEGIS experiment and subsequently to propose a solution to the injection of positrons into the main part of the apparatus. The result of this work is a proposal of the positron transfer line which will guide positrons from the positron accumulator into the main magnet. Positrons are guided and radially confined by axial magnetic field created by the main guiding coils of the transfer line. To perform track corrections pairs of racetrack coils in Helmholtz geometry are surrounding the main coils. An overview of AEGIS experiment is also provided in this work. In particular antiproton cooling methods and the gravitational measurement in AEGIS are outlined.

Key words: antihydrogen, AEGIS, antiparticle cooling, positron transfer, gravitational measurement.

Acknowledgments

I would like to thank to doc. RNDr. Vojtěch Petráček CSc. for being a kind and helpful supervisor that introduced me to the exceptionally interesting field of experimental antimatter research and supported me in my work. Also I would like to thank everybody from INFN Genova for their warm reception and especially I am very grateful to Gemma Testera for her expert guidance and for the fruitful discussions that we had. Thanks go to Alexey Dudarev for helping me out with the transfer line coils. Furthermore, I want to thank Johanka Borovanská for her support and patience and I am grateful to Radek Šmakal for help and to Miro Krůs for exceptional scholastic support throughout my studies.

Last but not least, I must thank my parents for their boundless support.

Contents

1	Introduction	5
2	Motivation of AEGIS	6
3	Antihydrogen formation and acceleration in AEGIS	8
3.1	Antihydrogen formation mechanisms	8
3.2	Stark acceleration of Rydberg antihydrogen	9
4	AEGIS apparatus	13
4.1	Antiproton decelerator	13
4.2	Positron accumulator	14
4.3	Main magnets and cryostat	16
4.4	Dilution refrigerator	18
4.5	Antiproton and positron traps	20
5	Antiproton cooling and plasma compression techniques	25
5.1	Antiproton cooling with preloaded electron cloud	25
5.2	Particle motion in Penning traps	27
5.3	Sideband cooling	28
5.4	Rotating wall technique	29
5.5	Resistive cooling	30
5.6	Antiproton laser cooling via negative ions - the UNIC project . .	32
6	Positron transfer in AEGIS	33
6.1	Requirements on the positron transfer	33
6.2	e^+ injection through the central region	34
6.3	e^+ injection from the AD side	34
6.4	Positron transfer line proposal	37
7	Gravity measurement	42
7.1	Classical Moiré deflectometer	42
7.2	AEGIS Moiré deflectometer and the gravity measurement	43
8	Beyond the first measurement	49
8.1	Trapping and cooling of antihydrogen	49
8.2	Improved gravity measurement using atom interferometry	50
8.3	Antihydrogen spectroscopy and CPT invariance	50
9	Conclusion	51

1 Introduction

The Antimatter Experiment: Gravity, Interferometry and Spectroscopy (AEGIS) is a new experiment primary goal of which is to measure the Earth's gravitational acceleration g on antihydrogen. The experiment will be located at the world's unique Antiproton decelerator at CERN which delivers slow antiprotons for antimatter research. The AEGIS experiment was recently (December 2008) approved by the CERN research board and technical design specification of the experiment along with the necessary simulations are currently being undertaken by the members of the collaboration [1].

The objectives of this thesis were contributing to the final design of the AEGIS experiment. The objectives were:

- To make simulations of the positron movement in the magnetic field of the experiment.
- To offer a proposal on the positron injection into the experiment.

In order to complete the objectives I had to learn new simulation techniques with the OPERA 3D software and overcome the obstacles imposed by other parts of the experiment. I have spent one month at INFN Genova where I worked on the positron injection under the guidance of Gemma Testera and her colleagues. The objectives of this thesis were exceeded. Based on the performed simulations, the positron transfer line - a solution that I had proposed - was accepted by the AEGIS collaboration and after a lengthy optimization I had successfully presented a detailed plan and a cost estimate at the AEGIS collaboration meeting. The results of my work are described in Section 6.

This work was my first encounter with antimatter experimental physics hence this thesis (aside from the positron transfer line description) gives also an overview of the whole experiment pinning out some crucial aspects and areas of my future interest. Since it was my first year studying the considerable number of experimental techniques used to produce antimatter, the work does not go into great detail on every subject, but tries to give a comprehensive overview of the planned AEGIS experiment.

In section 2 a brief physical motivation on the gravity measurement on antimatter is given. Section 3 presents the reaction mechanism of antihydrogen production along with the method of antihydrogen acceleration. In section 4 the setup of AEGIS with individual parts is described. In section 5 the methods of cooling of antiprotons down to mK range (and maybe even lower) are presented. The gravity measurement methods along with the explanation of the Moiré deflectometer are given in the section 7 and finally there is a short section 8 devoted to the future possible applications of the AEGIS apparatus.

2 Motivation of AEGIS

During the first phase of AEGIS experiment a 1% precision measurement of the gravitational acceleration is being expected. Even though this seems rather a low precision measurement it incorporates state-of-the-art techniques and there is a reasonable research and development done to improve antihydrogen production methods compared to AEGIS predecessor - the ATHENA experiment [5]. In addition new techniques in antihydrogen production and cooling will be used.

The gravitational interaction of matter and antimatter is expected to be the same (especially at 1% level), nevertheless various theories that do allow for differences between gravitational interaction on matter and antimatter. As pointed out by Goldman et al. [2] a broad range of quantum gravity theories introduce a finite range (Yukawa-type) interaction potentials that have approximately gravitational strength. In those theories gravivector (spin-1) and graviscalar (spin-0) components of the gravitational interaction are allowed (in addition to graviton with spin-2). Based on those theories (in a static simplified case) the total gravitational interaction energy between two fermionic massive objects is governed by:

$$V(r) = -\frac{Gm_1m_2}{2} \left(1 \mp ae^{-r/v} + be^{-r/s} \right), \quad (1)$$

where r is the distance between the objects, m_1 and m_2 are their masses and a and b are the products of vector and scalar charges of the particles and v and s are the inverse masses of the graviphoton (vector) and graviscalar [2]. The sign in front of a from Eq. 1 is negative in the case of matter and matter interaction. Models of these interactions were constructed so that the two new (Yukawa-type) components in Eq. 1 cancel out (based on the observations made so far). The interest in Eq. 1 to AEGIS lies in the case of matter antimatter interaction where the sign in front of a changes and the two new components add-up, thus based on these theories the antihydrogen should experience greater acceleration than ordinary matter. Goldman et al. even assume that if $a \sim b \sim 1$; quantum gravitational effect would make the antiprotons fall by a few percent faster than protons [3]. These theories of course violate the weak equivalence principle (WEP) which states that the inertial and gravitational masses are the same.

The above arguments illustrate just some experimental motivation for AEGIS' primary goal. There are many other interesting theoretical assumptions waiting to be confirmed by the gravitational measurement on antimatter [4]. The measurement of the gravitational acceleration between matter and antimatter in AEGIS is free of any assumptions and even the violation of WEP would be consistent with the CPT invariance¹.

Antihydrogen is composed of antiproton and positron (the counterparts to proton and electron); thus one might argue that for gravitaional measurement the 1840 times lighter positron does not play any role. There have been some experiments [3] performed on antiprotons trying to measure their gravitational interaction with Earth, but all failed due to large systematic errors. Even small fringing electromagnetic field acting on a charge overwhelms the gravitational force. Antihydrogen is neutral and thus it is affected only by magnetic and elec-

¹since CPT says that matter with matter interaction must be the same as antimatter with antimatter, but does not constrain matter-antimatter interaction

tic dipole interaction. In addition since the atoms are not polar (as opposed to some molecules) the electric dipole effect is in regular electric fields insignificant.

The AEGIS apparatus should make it possible to perform other fundamental tests with antimatter in a second phase of the experiment which is expected to be undertaken once the first gravity measurement is successfully achieved (2013). In the second phase of the experiment antihydrogen trapping is envisaged with subsequent cooling; that might lead to atom interferometric (higher precision) gravity measurement. Under the same conditions (trapped and cool \bar{H}) it would be possible to perform spectroscopic measurements to test the CPT invariance. The goals and methods of the second phase of the experiment are described in Sec. 8.

3 Antihydrogen formation and acceleration in AEGIS

The AEGIS experiment is based on the experience gained in the previous antimatter experiments at the CERN Antiproton Decelerator (further on AD). A major part of the current AEGIS collaboration is coming from the ATHENA experiment ([6] and [5]), which along with the ATRAP experiment [7] were the first to create and observe the formation of cold antihydrogen by using electromagnetic traps.

The particle manipulation techniques prior to the antihydrogen formation are similar in the AEGIS, ATRAP and ATHENA experiments. First, the positrons are stored for approx. 300s using a positron accumulator with a ^{22}Na β^+ source (see section 4.2), then they are transferred into the 3-6T magnet, where they are cooled by the emission of synchrotron radiation. Second, the antiprotons coming from the AD are degraded (slowed down) by a series of foils so that they could be trapped in the penning traps located in the main 3-6T magnet. The antiprotons are sympathetically cooled down by a preloaded electron cloud, that in turn cools itself down via the emission of synchrotron radiation.

3.1 Antihydrogen formation mechanisms

So far the techniques proposed are known and similar to the other experiments, but in AEGIS a different approach is used for the antihydrogen formation. The formation of antihydrogen in AEGIS is based on the charge exchange reaction between a Rydberg (a highly excited state) positronium² and an antiproton

$$(e^+e^-)^* + \bar{p} = \bar{H}^* + e^- \quad (2)$$

The charge exchange reaction used for the formation of cold antihydrogen was pioneered by C.H.Storry et al. [8] at ATRAP. The difference between ATRAP and AEGIS lies in the positronium formation. In ATRAP a reaction of Cesium atom with positron is used for the creation of positronium. Cesium is excited by laser and flies into a cloud of positrons, thus creating Cs ion and a positronium

$$\text{Cs}^* + e^+ \rightarrow \text{Cs}^+ + (e^+e^-) \quad (3)$$

which flies into the antiproton trap and produces antihydrogen. In AEGIS the positronium is created by impacting the cloud of positrons onto a porous cold target (Fig. 1). The specific material that is to be used is currently under experimental study; so far silica targets seem to be a good choice with yields close to 30%.

In ATHENA the antihydrogen atoms were created in a nested penning trap shown in Fig. 2, where the antiprotons were confined with the positrons in the same space and were let to recombine with positrons in a nested well. In ATHENA the main antihydrogen production process was through three body recombination reaction

$$e^+ + e^+ + \bar{p} = \bar{H} + e^+, \quad (4)$$

where the created antihydrogen atom occupies highly excited states.

²a bounded state of positron and electron

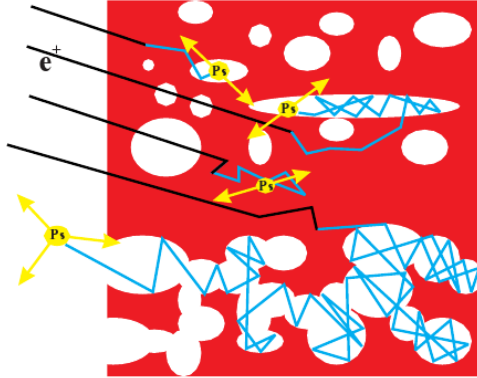


Figure 1: Positronium is formed at high yields when impacting on porous films [9]

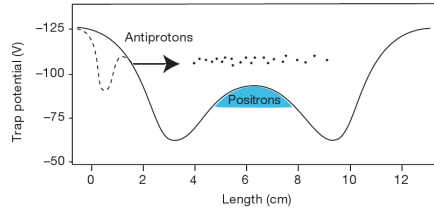


Figure 2: The nested penning trap scheme used for antihydrogen production in ATHENA experiment; along x is the length of the trap, along y is the applied voltage in the trap. [36]

The charge exchange reaction with positronium has many positives when being compared to the classical mixing technique used in the ATHENA experiment. Reaction (2) has a large cross section of the order of $a_0 n^4$, where $a_0 = 0.05 nm$ is the Bohr radius and n is the principal quantum number of the positronium. Also the resulting distribution of the formed antihydrogen is similar to the distribution of the quantum states of the positronium that formed it. This will be used in AEGIS, as the positronium atoms travel towards the antiproton trap they will be excited by two laser pulses (tunable) into the required states. In this way the antihydrogen atoms will be created at relatively narrow band of highly excited (Rydberg) states. Such pulse production (approx. every 300s) of antihydrogen atoms that are in distinct Rydberg states is favorable for the Stark acceleration of neutral antiatoms.

3.2 Stark acceleration of Rydberg antihydrogen

The main experimental challenge of AEGIS is the preparation of a beam of neutral antimatter. There are many technical obstacles that need to be overcome in order to prepare such a beam. Some of them have already been pointed out, such as the formation and excitation of positronium and also the antihydrogen formation by charge exchange. After (not only) these milestones are fulfilled it is crucial to accelerate the newly formed antihydrogen in a controlled way onto

the Moiré gratings to perform the gravity measurement.

The deceleration and acceleration of neutral matter was already experimentally demonstrated by groups at University of Oxford [10] and at ETH Zurich [11]. The ETH group (which is part of the AEGIS collaboration) had also done quite recent experiments with decelerating and trapping Rydberg hydrogen atoms [12]. The principle of Stark acceleration or deceleration of neutral atoms is based on the conversion of potential to kinetic energy as a particle with large electric dipole moves in an inhomogeneous electric field. The Stark acceleration is an electrical analogue to the Stern-Gerlach experiment.

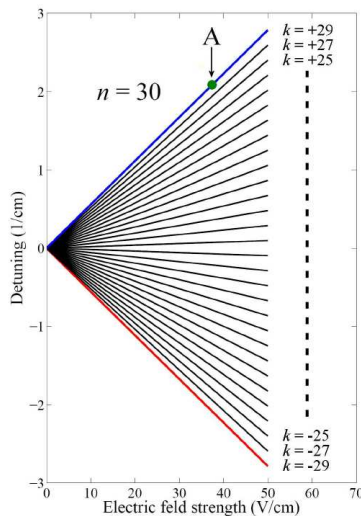


Figure 3: The Stark states of Rydberg hydrogen with $n = 30$ and $m_l = 0$ plotted as a function of electric field strength. On the vertical axis is the detuning from the energy of Rydberg hydrogen in field free region. [4]

The energy of H atom in an electric field F is (in atomic units, to the first order approximation [11]):

$$E = -\frac{1}{2n^2} + \frac{2}{3}nkF, \quad (5)$$

where k is a quantum number running in steps of 2 from $-(n - 1 - |m_l|)$ to $(n - 1 - |m_l|)$ and m_l is the azimuthal quantum number.

To show how the electric field can accelerate and decelerate lets look at a case of hydrogen atom in a $n = 30$ and $m_l = 0$ state (taken from [4]). A picture of the allowed Rydberg Stark states for such atom is in the Fig. 3, the states are plotted as a function of electric field strength. If we have an atom in a state with high positive k value (for example the one drawn A in the Fig. 3) and it is moving towards higher electric field region, its potential energy increases and the atom decelerates (so that the total energy is conserved). Such an atom is in the so-called low-field seeking state³. Vice versa, if we have an atom at a high-field seeking state (k being negative) it would get accelerated during the

³As if the atom would like to go back to the lower field region where it came from.

travel towards a higher electric field. Having an atom in one principal quantum state n , the change in energy (following the equation (5)) is

$$\Delta E = \frac{2}{3}nk\Delta F \quad (6)$$

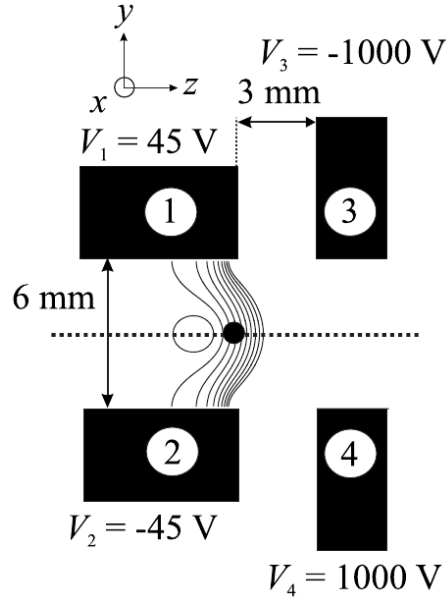


Figure 4: Electrodes schematic setup during Rydberg hydrogen deceleration prior to hydrogen trapping at ETH [12].

The experimental setup for deceleration and trapping of Rydberg hydrogen performed at ETH Zurich is shown in Fig. 4. In this experiment the Rydberg hydrogen atoms at initial velocities of ≈ 750 m/s were stopped in a distance of less than 3 mm. To achieve this a voltage pulse of 1 kV with sharp rise time and decay of approx. $10 \mu\text{s}$ was applied to the electrodes 3 and 4 (in Fig. 4) at opposing polarities ($V_3 = -V_4$). A similar scheme is anticipated in AEGIS with the main difference that the electrodes will not have a rectangular shape as in the case of the above mentioned experiments, but will be in form of segmented (electrically split) cylinders that quickly change polarities from Penning-type trap into an atom Stark accelerator. In AEGIS the goal will be to accelerate the cold and isotropically spreading cloud of antiatoms onto the Moiré gratings located at the exit from the magnet.

There is another novelty in the Rydberg acceleration on antihydrogen. The previously mentioned experiments were not done in the presence of strong magnetic field. In AEGIS the antihydrogen is created in a Penning trap (sec. 4.5) where the fields are in the range between 1 and 6 T. For (charged) particle trapping it is convenient to have higher axial fields. Unfortunately the dynamics of Rydberg atoms in arbitrarily crossed magnetic and electric fields is a complex problem. According to Main et al. [13] there are many different regimes of classical motion depending on a range of parameters (like the angle between the fields, their strength, the principal quantum number). When the mutual angle between

the fields is from 40° to 70° , the classical motion might even become chaotic. The effect of energy levels splitting under strong magnetic fields also plays an important role in the dynamics of excited atoms. Large perturbations of the Rydberg antihydrogen are unwanted thus a compromise was chosen between the field in the trap and the requirement to not perturb the antihydrogen via strong fields. The perturbations are caused by the linear and quadratic Zeeman terms. A compromise was chosen to have 1T field in the formation/acceleration region along with maximum principal quantum number of antihydrogen $n=35$. The regime during which formation and acceleration of antihydrogen will take place will be the so-called weak field regime when the linear Zeeman effect is stronger than the quadratic one.

4 AEGIS apparatus

In this section the AEGIS experiment with its various parts is described. All the components of the experiment play an important role in achieving the scientific goal. Research and development on many of those components is currently in progress; once the construction starts many parts of the apparatus might be quite different from those presented in this overview. Since the positron transfer was the main objective of this thesis it is described in a separate section 6. The AEGIS experiment will be located in the AD6 zone at the CERN Antiproton Decelerator (further on AD) and even though AD it is not an integral part of AEGIS a brief description of this unique device will be given in the section 4.1.

An overall layout of the experiment in the zone is shown in Fig. 5. Antiprotons are coming from the AD on the (so-called main) axis of the 5T and 1T superconducting magnets. The magnets are housed in a 4.2K cryostat which ends with a 77K chamber housing the Moiré deflectometer gratings with the position sensitive detector. The positron accumulator - the source of positrons for the experiment - is located above the antiproton beam line. In the zone there is also space for laser tables needed for efficient positronium excitation or for perspective antihydrogen cooling. On the side of the zone there are the racks for all the needed instrumentation.

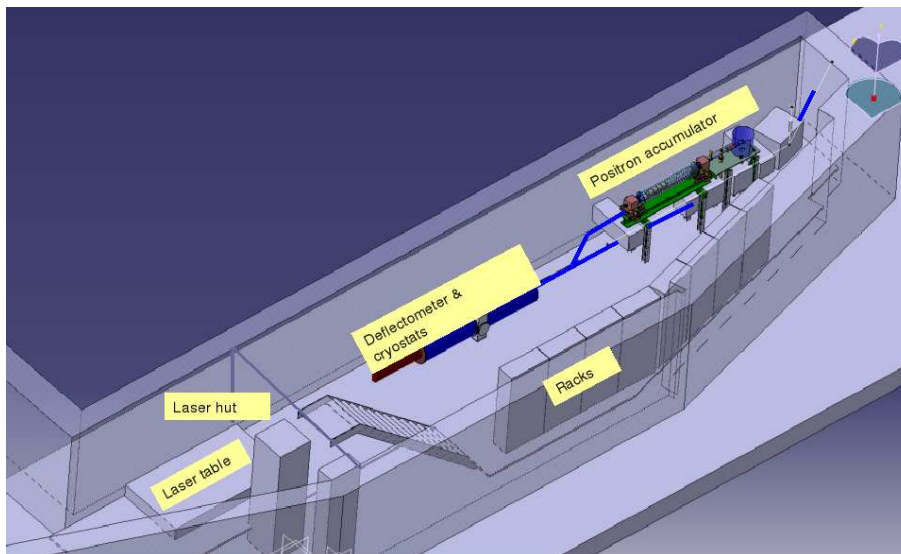


Figure 5: The layout of the AEGIS apparatus in the AD6 zone at the CERN Antiproton Decelerator

4.1 Antiproton decelerator

To produce antihydrogen one needs antiproton \bar{p} and positron e^+ . Positrons are most conveniently formed in β^+ decays of unstable nuclides, but there are no radioactive emitters of antiprotons available. The antiprotons are produced in collisions of accelerated protons (at GeV kinetic energies) with a fixed target. At CERN 26GeV protons are accelerated by the Proton Synchrotron and left

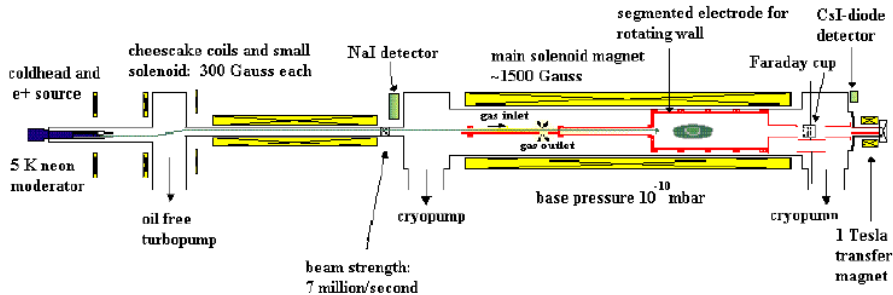


Figure 6: A detailed schematic view of the positron accumulator of the ATHENA experiment. [15]

to collide with a target in which the antiprotons are produced. They are then extracted and slowed down at high efficiency by the Antiproton Decelerator (AD).

Empirically the highest yield of antiprotons is at output energy of 3.57 GeV (with protons being at 26 GeV). Approximately $5 \cdot 10^7 \bar{p}$ are extracted and guided into the decelerator ring. The decelerator is similar in construction to an accelerator with the difference being that the acceleration RF cavities are used to slow down the beam. This brings in the main difficulties. When the bunch slows down its dispersion or emittance increases (since we reduce the forward velocity only). In addition the emittance of the incoming primary beam is not too good (around $200\pi \text{ mm.mrad}$). To improve the momentum dispersion of the incoming beam the bunch rotation is applied, thus reducing the dispersion from $\pm 3\%$ to $\pm 0.75\%$. To improve the antiprotons transverse dispersion Stochastic cooling method is applied, after which their transverse spread is $5\pi \text{ mm.mrad}$ and momentum spread only 0.1%. Then they are slowed down to 2 GeV and stochastically cooled again. In the next stages electron cooling is applied which is suitable for lower energy beam cooling. The AD finishes the cycle by delivering 5.3 MeV ($100 \text{ MeV}/c$) antiprotons with transverse beam emittance of $1\pi \text{ mm.mrad}$ and momentum spread of 0.1%. The whole cycle of the deceleration takes approx. 100s with $\sim 2.5 \cdot 10^7$ antiprotons delivered to the experiments at the AD experimental hall.

4.2 Positron accumulator

To produce antimatter one also needs the positrons. A standard technique used in the antimatter experiments is the accumulation of positrons coming from a radioactive β^+ source. In AEGIS the same type of device as in ATHENA would be used - the so-called Surko type positron accumulator⁴ - which is now available commercially.

A schematic picture of the ATHENA positron accumulator is in Fig. 6. This accumulator was the first to use the rotating-wall technique to cool down and compress the positron plasma; its optimization is thoroughly presented in doctorate thesis of T. Watson [15]. The positrons are produced by a $50 \text{ mCu } ^{22}\text{Na}$

⁴Prof. C.M. Surko's positron research group at the University of California, San Diego pioneered these types of accumulators.

β^+ source. Since the beta decay energy spectrum has a mean yield value in the MeV range, for low energy experiments a moderation technique to slow down the positrons is being used. There have been many different types of moderators used in the past, currently the solid Neon moderator has the highest efficiency in positron moderation. The radioactive sodium source is mounted on a cold (cryogenic) head at temperature around 5K, on which Neon gas is let to desublimite and grow a layer of ideal (experimentally tested) thickness. The effect of such moderation is shown in the next Figure 7. Even though the efficiency of

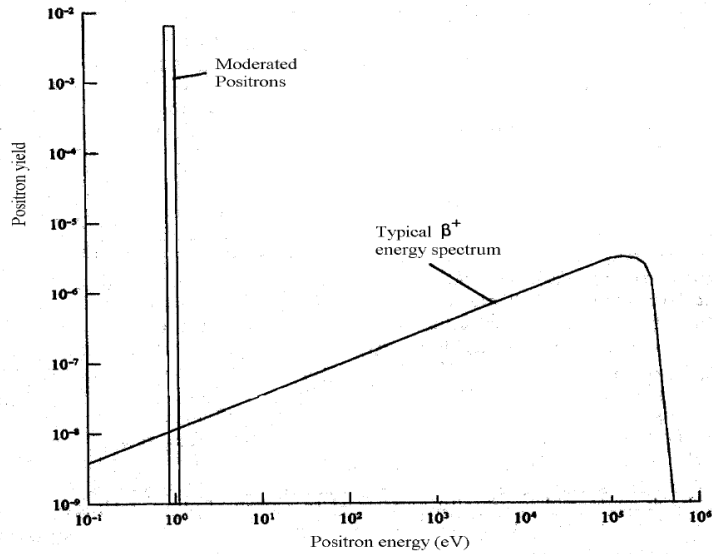


Figure 7: The β^+ energy spectrum before and after solid neon moderation. [15]

such moderation is $7 \cdot 10^{-3}$ the resultant spectrum is very narrow and suitable for low energy trapping and cooling techniques. The source chamber is being pumped by oil-free turbo pump (there is a risk of moderator contamination) and divided from the trapping region by a long and narrow vacuum chamber, acting as a pumping restriction.

Once moderated the positrons fly through the narrow tube into the main trapping region where Nitrogen buffer gas and Penning-Malmberg traps are located⁵. Here the accumulation process takes place. This region is surrounded by 0.15T water cooled coil which axially confines the positrons. In order to trap the incoming positrons they need to lose sufficient amount of energy during their passage through the trap system so that they would not go over the entrance electrode voltage barrier. A buffer N_2 gas is being used to slow positrons down via inelastic collisions of positrons and Nitrogen molecules in which positron has a kinetic energy in the range $\approx 7 - 11\text{eV}$, that is high enough to excite electronic transitions in Nitrogen molecule, but not too high to form positronium.

⁵Penning traps are made from concentric cylindrical electrodes with axial magnetic field. The magnetic field confines the particles radially while electrostatic field at the end cylinders confines the particles in the axial direction. Originally designed by F.M. Penning as a vacuum gauge (the PIG or the Phillips Ion Gauge) it came to be used extensively as an ion source and also as a charged particle trap. For more details see Sec. 4.5 and Sec. 5.2.

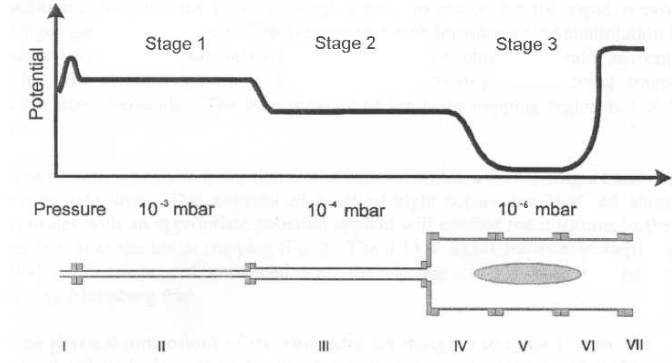


Figure 8: A schematic of the traps in the positron accumulator main trapping region with potentials, pressures and electrode dimensions. [15]

Fig. 8 shows schematically the trap dimensions, pressures and the applied potentials in positron accumulator. The differential pumping scheme allows the efficient trapping. As a positron gets gradually slowed down by many collisions with the buffer gas it moves one stage lower (in the potential view) and finally ends up in the last 10^{-6} mbar pressure region. Here the positrons are being accumulated and also compressed by the rotating wall technique (5.4), which will be used also for the antiprotons and positrons in the main 5T and 1T magnets. Annihilation of positrons is higher in the high pressure regions; the gradient of pressures (see Fig. 8) was experimentally chosen as to maximize the positron accumulation. At the end of the accumulation (after approx. 300s) there should be approx. 1.5×10^8 positrons ready for transfer into the main magnet. The accumulation and annihilation of positrons in the buffer gas are competing processes that is why a saturation effect is seen. In Fig. 9 we can see the the measured number of accumulated positrons as a function of time for the ATHENA positron accumulator. The number of accumulated positrons was measured by dumping the accumulated e^+ cloud on a Faraday cup and (complementary) measuring the annihilations with a CsI crystal (Fig. 6). The maximum accumulation occurs at around 300s afterward a sligth decrease is apparent for both measurements.

4.3 Main magnets and cryostat

As we can see in the layout (Fig. 5) the cryostat is located in the middle of the zone on the antiproton beam line axis. Inside the cryostat there are three important components of the AEGIS design: the two superconducting magnets and the dilution refrigerator - a device capable of achieving temperatures below the 4.2K liquid ^4He limit. A picture of the planned AEGIS cryostat is in Fig. 10. Going from the left to right, there is the 5T superconducting magnet with the antiproton and positron catching traps. In the middle there is the central instrumentation region, where the dilution refrigerator (capable of achieving 100mK), as well as the diagnostics and the laser windows are located. The right part of the cryostat is housing the 1T magnet with the antihydrogen formation region and finally there is the 77K liquid nitrogen thermal shield which covers

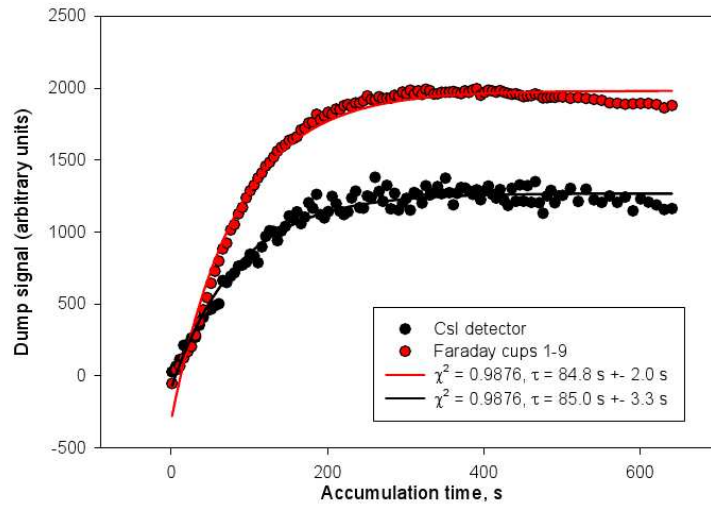


Figure 9: The accumulation of positrons as a function of time; measured at the ATHENA positron accumulator. [15]

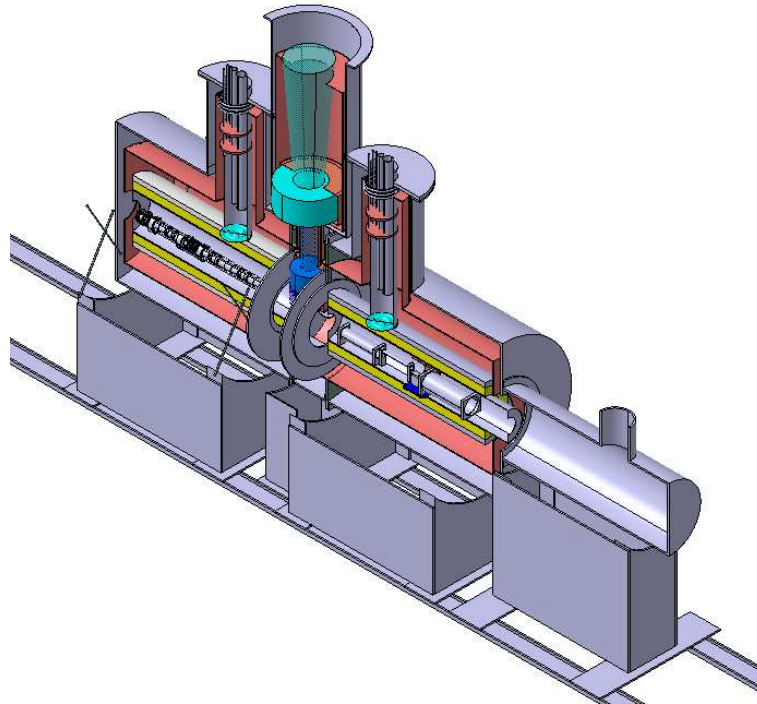


Figure 10: The AEGIS cryostat housing the superconducting (5 and 1T) magnets, the dilution refrigerator (0.1K capable) and the 77K thermal shield around the gratings and detector chamber.

the gravity measurement region.

The 5T magnet is a coil with windings made from superconducting alloy; the AEGIS 5T magnet has to have a homogeneity of 10^{-4} in a length of approx. 30cm in the centre of the coil in order to achieve long antiproton and positron storage times. In the 5T magnet there will be the antiproton catching and cooling trap and the positron cooling trap. The 1T magnet is similar in construction to the 5T one however its magnetic field will be lower. This magnet is housing one of the critical parts of the experiment - the antihydrogen formation region with ambient temperature of 100mK and the positronium formation target. As discussed in section 3.2 the field of 1T is a compromise between the long particle storage times and the Rydberg antihydrogen perturbations. Since the field is only 1T, this magnet needs to reach a homogeneity better than 10^{-5} in order to achieve sufficient plasma storage times. Both of the magnets will have an anticoil at their end so that their fringing field can be reduced (this will be of special interest for the gravity measurement region).

4.4 Dilution refrigerator

A dilution refrigerator capable of achieving 100mK temperature is being built at CERN. It will be located in the central instrumentation region of the cryostat (Fig. 10). The lowest temperature will be achieved in the centre of the 1T magnet in the so-called mixing chamber. The principle of dilution refrigerator can be understood from the phase diagram of liquid helium mixture (mixture of helium-3 and helium-4) shown in Fig. 11. Helium-4 is liquid below 4.2K (at

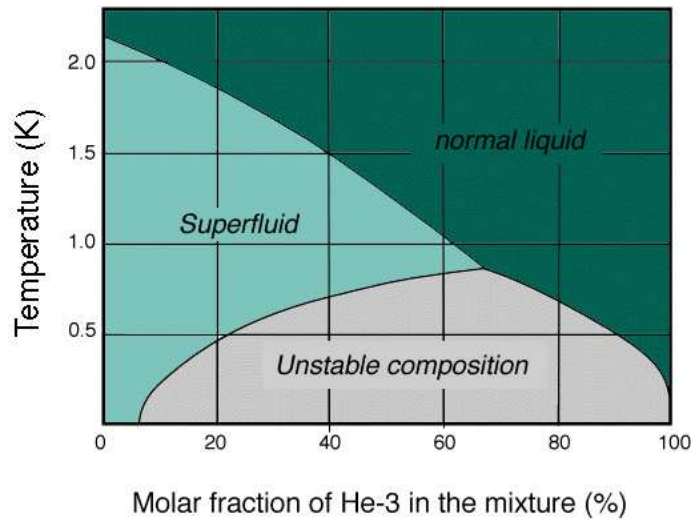


Figure 11: The phase diagram of liquid helium mixture (^3He and ^4He) at low temperatures.[16]

normal pressure) and becomes superfluid below 2.17K. When we have a mixture of the two helium isotopes below 0.86K (the triple point in Fig. 11) it separates into two phases: the He-3 rich phase and the He-3 poor phase. When lower the

temperature, we move along the equilibrium line either to the right from the triple point (rich phase) or along the line to the left (the poor phase). Even at absolute zero the concentration of He-3 in the poor phase is finite at 6.4%.

Below 0.5K the superfluid He-4 has negligible entropy and behaves like a vacuum to the He-3 atoms. In the mixing chamber the ultimate cooling takes place. Here the two phases are together; the rich phase is lighter and "sits" above the poor phase (which is heavier due larger He-4 concentration). He-3 atoms are made to cross the boundary between the phases in the mixing chamber by pumping on the still (Fig. 12) which is located further up at a temperature slightly below 1K (where the He-3 evaporates). The still is connected to the poor phase and since we pump mostly He-3 we destroy the 6.4% (at least) equilibrium in the poor phase. In order to restore the equilibrium He-3 atoms cross the phase boundary. To do so they acquire energy from the mixing chamber walls. By using the dilution refrigerator temperatures around 2mK ([17]) can be achieved.

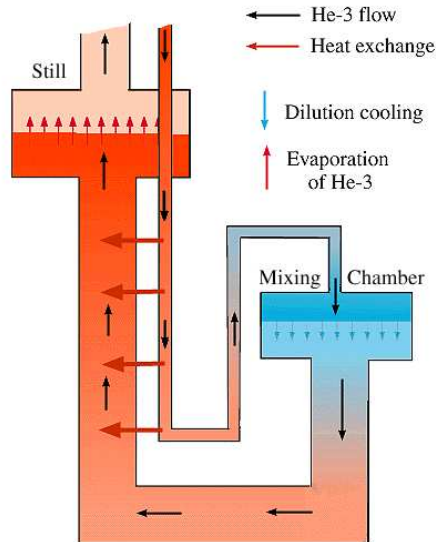


Figure 12: A schematic of a dilution refrigerator. [18]

The dilution refrigerator of AEGIS will have a cooling power of approx. $500\mu W$ at 100mK temperature. The mixing chamber will be located beneath the antihydrogen formation trap and connected to the rest of the dilution refrigerator via two tubes. The mixing chamber is also specially designed for the AEGIS antiproton and electron traps (Fig. 13).

All of the ultra-cold components will be isolated by many layers of thermal insulation. The main heat load in the antihydrogen formation region will be coming from the thermal radiation of the warm areas (4.2K, 77K and even some 300K room temperature radiation). Other heat loads will be coming from the cables driving the trap voltages and also from the lasers that are needed to excite the positronium prior to charge exchange reaction. Even though the lasers would go through the chamber (thus exiting the apparatus) substantial heat load will be deposited in the formation region.

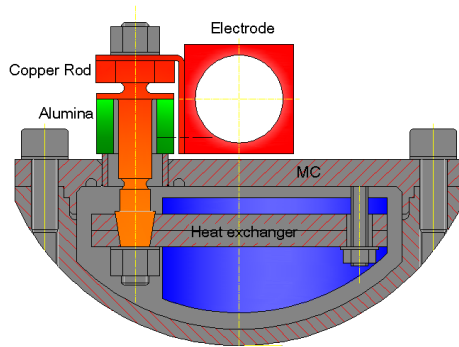


Figure 13: The 100mK mixing chamber of the AEGIS dilution refrigerator

4.5 Antiproton and positron traps

Antiprotons and positrons will be caught and stored in Penning-Malmberg traps situated inside the 5T and 1T magnets. These traps consisting of cylindrical electrodes (Fig. 14) are well known and extensively used for charged particles and non-neutral plasma storage experiments. The axial magnetic field confines the particles radially while the end electrodes create an electrostatic potential well that traps the particles axially. Penning type trap has a harmonic potential while in Penning-Malmberg trap the central electrode is longer, thus creating a different trapping potential shape (Fig. 14). Stacking, storing and compression of the non-neutral plasmas is being enabled by the trap electrodes which are segmented in radial and longitudinal directions. The techniques of antiproton and positron cooling and manipulation are described in detail in section 5.

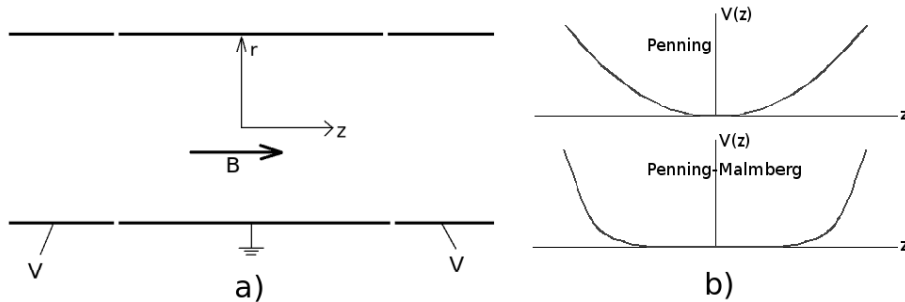


Figure 14: A schematic of a penning trap (a); the axial magnetic field confines the particles radially while the end electrodes confine the particles in an electrostatic potential well axially. In (b) the potential along the trap axis for Penning and Penning-Malmberg trap is schematically depicted.

In AEGIS the trap system will be located along the whole length of the superconducting magnets. In the 5T magnet there will be one trap located on the main axis used for antiproton and positron catching and cooling. Such trap is depicted in Fig. 15. The first part of the trap (left side in Fig. 15) is used for catching of positrons and antiprotons; this part has two high voltage electrodes

used for antiproton catching. After the antiprotons had been slowed down in the degrader foil (located at the entrance to the catching trap) they pass the entrance electrode which is on ground potential, whilst the second high voltage electrode is at approx. 10kV. The antiprotons below 10keV bounce back, but during this time a fast 10kV pulse is applied on the entrance electrode causing the trap to close down. The positrons are caught after their transfer from the positron accumulator in a similar way (at lower and thus easier achievable voltages). The second part of the 5T trap (Fig. 15) consists of the positron

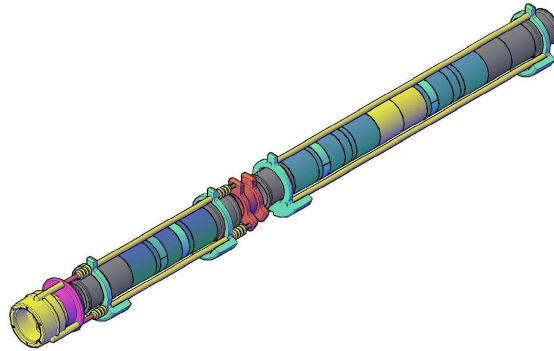


Figure 15: The antiproton and positron catching and cooling trap located in the 5T magnetic field; left side - the catching trap, right side - storage, compression and diagnostics trap.

and antiproton storage and compression trap, where the already cooled down bunch of positrons or antiprotons is stored and compressed with the help of the rotating wall plasma compression method ([19] and Sec. 5.4). The diagnostics (of the shape and density) of the stored plasmas would be done by nondestructive plasma mode frequency measurements for which a harmonically shaped potential is needed (Penning trap).

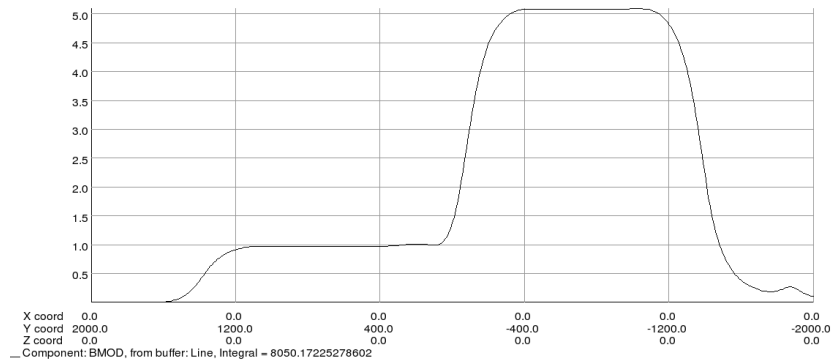


Figure 16: Magnetic field along the main axis of AEGIS (OPERA 3D); on the left 1T field, then the transfer section and on the right 5T magnet field. A small 0.3T bump on the right is the axial coil of the positron transfer line.

Between the 5T catching and cooling trap and the trap in the 1T antihydrogen formation region there will be a transfer region, where the field will drop from 5T to 1T (Fig. 16). This transfer region will be also filled with cylindrical electrodes and thus could be used as a Penning trap. But because of the lack of homogeneity the storage times of plasmas in this region would be shorter. Despite of the anticipated short storage times the transfer section (with a similar multi-electrode set-up as the catching trap) could be used for adiabatic (slowly changing neighbouring potentials) or ballistic positron/antiproton transfer into the 1T homogeneous region. In the ballistic transfer method the cloud of charged particles is accelerated to higher (tens or hundreds eV) kinetic energies and caught in the region of interest using the same principle as for antiprotons in the 5T catching trap.

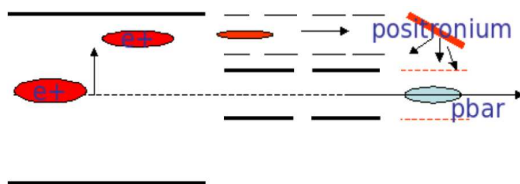


Figure 17: A schematic of the 1T big trap, that is divided into two small traps in the 100mK region; small axial for antiprotons; small off-axis for positrons and positronium target.

In the 1T region (where the antihydrogen production takes place) the trap layout is different from the 5T one. Here the antiprotons or positrons will (at different times of course) arrive into the 1T homogeneous field where a trap with bigger radius (due to the plasma expansion in weaker axial field) will be located. The trap radius of the 5T catching trap will be of the order of 1.5cm whereas in the 1T big trap the radius will be around 2.5cm. The 1T trap schematic is shown in Figure 17, where the positron/antiprotons are coming from the left (transfer region) on axis. Two smaller traps that both fit within the radius of the big trap are located in the region of the highest homogeneity of at least 10^{-5} ; they are the antihydrogen formation traps. For the storage of antiprotons a small trap is located on the axis, while the other one is located off-axis and suited for positrons. A small positron trap will be followed by the positronium formation target (section 3.1) oriented in a slanted direction towards the antiproton small trap, which will have semi-transparent electrode to allow positronium passage. While the big trap will be at the temperature of liquid helium (at 4.2K) the small traps will be at the 100mK temperature. The mixing chamber of the dilution refrigerator (sec 4.3) will be located directly beneath them and thermally connected to them by copper rods. The small antiproton trap functions as the antihydrogen formation region and also as the Stark accelerator. Its electrodes are segmented and shaped in that respect. The mixing chamber of the dilution refrigerator is specially designed and tested, so that high voltage discharges could not occur in the helium mixture (Fig. 13). In the off axis trap the positron cloud will be compressed via rotating wall technique or sideband cooling in order to achieve radius of the positron cloud ≈ 1 mm. This compressed positron cloud will then be accelerated at variable energies (up to several keV - depending on the experimental observations on the

positronium formation) toward the positronium formation target.

When transferring the positrons from the 5T region into the 1T big trap, they end up on the axis; in order to inject them into the off-axis small positron trap one has to make them move across the confining axial magnetic field. This can be done within the Penning trap with the induction of diocotron motion of the positron plasma by applying a sine voltage signal with varying frequency (rising) on one (radial) segment of the electrode. The diocotron motion of plasma was recently applied experimentally during the development of a new generation of positron accumulators which should be capable of accumulating and storing 10^{11} positrons [20]. The above mentioned method allows to control the radial and azimuthal position of plasma in a Penning-Malmberg trap for relatively long times (thousands of diocotron periods). Inducing this motion enables to inject the positrons in a controlled manner into the off-axis trap. J.R. Danielson et al. show that during the induced radial motion of the electron cloud the plasma diameter stays almost constant (Figure 18). Thus the diocotron motion is an effective alternative either to magnetic field changes or to $E \times B$ drift methods. Assuming plasma has axial length large compared to the trap radius R_t , the linear frequency of the $m_\theta = 1, k_z = 0$ diocotron mode is

$$f_D \approx \left(\frac{r_p}{R_t} \right)^2 f_E, \quad (7)$$

where r_p is the plasma radius and f_E is the plasma $E \times B$ rotation frequency, dependent on the plasma density and magnetic field B through $f_E = (c n e) / B$. Normally the f_D is in the kHz range. Applying a sinusoidal voltage signal $V = V_0 \sin(2\pi f t)$ with variable (rising) frequency to one of the four radial segments of an electrode; one can displace the plasma radially by choosing the right final frequency f . In order to displace the plasma in a controlled way the starting driving frequency is chosen below the linear diocotron frequency (thus $f < f_D$). Then the driving frequency f is continuously increased until a needed displacement is reached. This displacement corresponds uniquely to the final frequency of the driving signal. This so-called autoresonance method leaves the plasma at fixed position in radial displacement and in phase. The experimental results of J.R. Danielson et al. [20] are shown in Fig. 18 and Fig. 19.

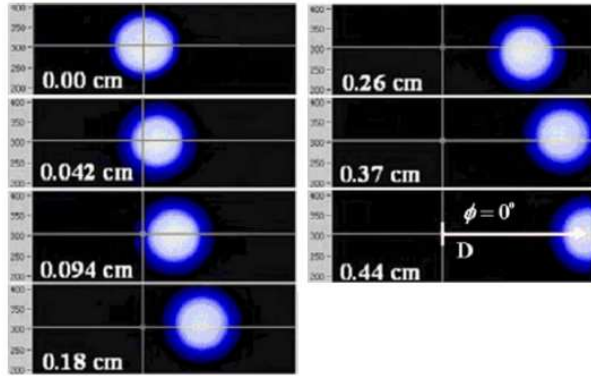


Figure 18: Images of plasma for different values of diocotron driving frequency f leaving the plasma at different displacement D (plasma dumped at the same phase $\phi = 0$). [20]

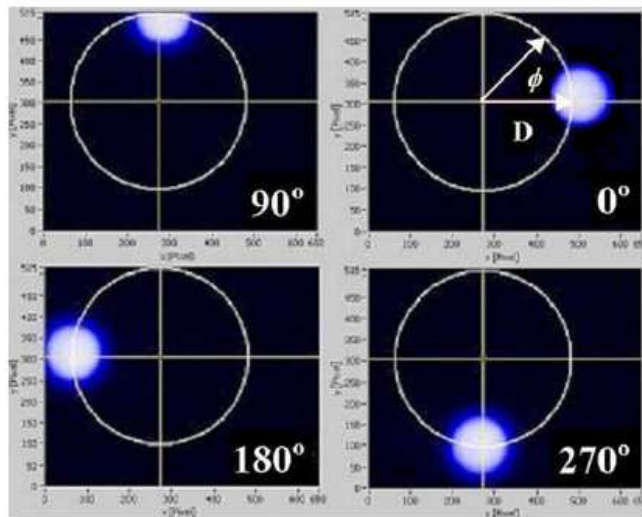


Figure 19: Images of plasma with displacement $D=0.26\text{cm}$ and at different phase angles ϕ . [20]

5 Antiproton cooling and plasma compression techniques

Antiprotons are coming from the AD at 5.3MeV. To stop and catch all of the 10^7 antiprotons one would need either to further decelerate them or to have a trap with end electrodes at MV potentials. This is of course technically unachievable, thus the already mentioned technique with a set of degrader foils is used by many antimatter experiments in the AD experimental hall. The degrader foils spread out the energy spectrum of the antiprotons to produce a reasonable number of antiprotons in the 0-10keV range which is suitable for catching. The efficiency of such deceleration method is tenuous. Out of the 2.5×10^7 antiprotons coming from the AD approx. 10^4 were captured by the 5kV potentials at the ATHENA catching trap [5]. To increase the catching efficiency it is planned to have trap electrodes at 10kV in AEGIS. Unfortunately since we are catching the far end of the antiproton energy spectrum by doubling the catching potentials we only double the number of antiprotons ; in this end region of the spectrum the curve can be approximated to be linear (as compared to its exponential behaviour in medium antiproton energies). Because of the low catching efficiency it is anticipated to stack more shots of antiprotons into the same catching trap (thus using more AD cycles for the accumulation of antiprotons). This was done in the ATHENA experiment and the number of accumulated antiprotons rises linearly with the number of stacked AD shots. The stacking will be done in a coordination with the positron accumulation, thus three to four shots of antiprotons are expected to be accumulated due to the approximate 300s accumulation time in the positron accumulator (Sec. 4.2).

5.1 Antiproton cooling with preloaded electron cloud

After the antiprotons have been caught the first cooling process takes place - the electron cooling. This cooling mechanism is sometimes also called the sympathetic cooling. The cooling of hot ions via Coulomb collisions with a cold cloud of electrons is a routine method used in the lower energy region starting from relativistic $\beta = 0.65$ downwards [23]. It is also routinely used in lower energy particle accelerators (storage rings) and it is a complementary method to the Stochastic cooling, which works better for higher particle energies. The main difference when using electron cooling of \bar{p} in a Penning trap lies in the fact that in accelerators we insert a constantly new high current and high quality e^- beam into the ion beam pipe opposed to the Penning trap where we pre-load an electron cloud and leave it confined in the same trap. In particle accelerators the new cold electron beam cools down the repeatedly incoming ions, while in the Penning traps we have the same electron cloud which cools itself via an emission of synchrotron radiation in the strong (in AEGIS 5T) axial magnetic field. Despite of those differences the principle of antiproton (ion) cooling is the same.

If we have a two-component nonneutral plasma where the components share the same volume and their temperatures differ, the relaxation (exchange in energy) takes place between them. The relaxation (electron cooling) time τ_c

can then be calculated using the so-called Spitzer equation [24]:

$$\tau_c = \left(\frac{3m_e}{8\sqrt{2}\pi e^4} \right) \left(\frac{m_p}{n_e Z^2 L_C} \right) \left(\frac{kT_p}{m_p} + \frac{kT_e}{m_e} \right)^{3/2}, \quad (8)$$

where m_e , T_e and m_p , T_p are the electron and antiproton masses and temperatures respectively, Z is the proton number (for antiprotons = 1), n_e is the electron density and L_C is the Coulomb logarithm.

A simple model of electron cooling is the binary collisional model, which assumes electron cloud to be stationary and ions (antiprotons) that fly through such cloud are scattered according to the Rutherford formula:

$$\frac{d\sigma}{d\Omega} = \left(\frac{Ze^2}{4\pi\epsilon_0 2m_p v_p^2} \right)^2 \frac{1}{\sin^4(\theta/2)} \quad (9)$$

where the $m_p v_p^2$ factor is the (non-relativistic) kinetic energy of the ion. Because of the $\sin^{-4}(\theta/2)$ term in eq. 9 small angle collisions are strongly favoured and thus the momentum approximation (to first order assuming undisturbed trajectory of the ion $x = v_p t$) is justified. Then the momentum transferred in an individual collision can be easily calculated from

$$\Delta p = \int_{-\infty}^{+\infty} F_C dt = \frac{1}{4\pi\epsilon_0} \int_{-\infty}^{+\infty} \frac{Ze^2}{x^2 + b^2} dt = \frac{1}{4\pi\epsilon_0} \frac{2Ze^2}{v_p b}, \quad (10)$$

where b is the impact parameter, v_p is the velocity of the incoming antiproton (Fig. 20) and F_C the Coulomb force. The energy lost in one collision is then

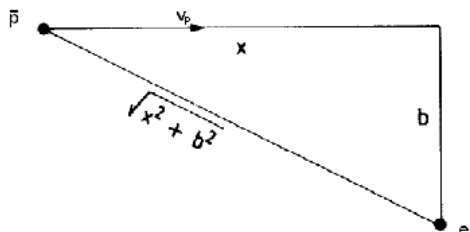


Figure 20: Kinematics of a binary collision during electron cooling (using the momentum approximation).

$\Delta E_1 = \Delta p/2m_p$ and the energy loss per length element dx of the antiproton to all electrons in a volume element $2\pi b db dx$ is

$$\frac{\Delta E}{dx} = 2\pi n_e b db \Delta E_1. \quad (11)$$

This equation shows the energy loss per length dx for impact parameter interval $(b, b + db)$ thus to get the energy loss when the antiproton passes the cloud of electrons we must integrate over the impact parameter b . To do the integration we need to have limits on the impact parameter. The maximum impact parameter b_{max} is given when taking into consideration the debye screening length of the electron plasma

$$b_{max} = \lambda_D = \sqrt{\frac{\epsilon_0 m_p v_p^2}{2e^2 n_e}}$$

The minimum impact parameter b_{min} is determined from the maximum momentum transfer that can occur (which is during a head-on collision)

$$\frac{1}{4\pi\epsilon_0} \frac{2Ze^2}{v_p b_{min}} = \Delta p_{max} = 2mv_p \rightarrow b_{min} = \frac{1}{4\pi\epsilon_0} \frac{Ze^2}{mv_p^2}$$

Integrating the eq. 11 we get the energy loss of antiproton as it passes through the electron cloud of density n_e

$$-\frac{dE}{dx} = 2\pi \int_{b_{min}}^{b_{max}} n_e b \Delta E_1 db = \frac{Z^2 e^4}{4\pi\epsilon_0 m_e v_p^2} \underbrace{\ln\left(\frac{b_{max}}{b_{min}}\right)}_{L_C}, \quad (12)$$

where we can see the Coulomb logarithm

$$L_C = \ln\left(\frac{4\pi}{Ze^3} \left[\frac{3\epsilon_0 kT}{2n_e}\right]^{3/2}\right).$$

Even though this model is very simple and not too exact eq. 12 shows the main feature of electron cooling techniques: the strong dependence of the antiproton (ion) energy loss on the v_p^{-2} . That is why the cooling rate increases substantially for lower energies of antiprotons.

The simple model of binary collisions is not exact, in order to get more precise results one has to take into considerations the velocity distributions of electrons and ions (antiprotons); a more precise model would also have to take into account the changes in the distributions. A more precise model for electron cooling is the Fokker-Planck theory of small angle collisions in a fully ionized plasma [23]. The electron cooling in AEGIS will be done by loading electrons coming out from an electron gun into a narrow potential well in the antiproton catching trap. The same technique was used in ATHENA experiment where nearly all antiprotons were cooled to eV range within 60s.

5.2 Particle motion in Penning traps

In an ideal Penning trap there is an axial magnetic field confining the particles radially and an electrostatic quadrupolar potential (in three dimensions) that confines the particles axially:

$$V = U_0 \frac{2z^2 - r^2}{2z_0^2 + r_0^2}, \quad (13)$$

where z_0 is the halflength of the trap in axial direction, r_0 is the radius of the trap and U_0 is the potential on the end electrodes. If we solve the classical motion of the particle in the above trap we obtain three types of harmonic motions that superimpose to form the overall motion of the particle in the trap [25]. There is one axial motion with axial frequency $\omega_z = \sqrt{4qU_0/[m(2z_0^2 + r_0^2)]}$ and phase ϕ_z

$$z = A_z \cos(\omega_z t + \phi_z).$$

And there are two radial motions which are described by vector equation:

$$\mathbf{r} = R_- \begin{bmatrix} \cos(\omega_- t - \phi_-) \\ -\sin(\omega_- t - \phi_-) \end{bmatrix} + R_+ \begin{bmatrix} \cos(\omega_+ t - \phi_+) \\ -\sin(\omega_+ t - \phi_+) \end{bmatrix},$$

and

$$\omega_{\pm} = \frac{1}{2}(\omega_c \pm \sqrt{\omega_c^2 - 2\omega_z^2}), \quad (14)$$

where the R_{\pm} are the amplitudes, ϕ_{\pm} are the phases and ω_{\pm} are the frequencies of radial motions. The minus underscore marks the so-called magnetron motion and the plus underscore marks the so-called modified cyclotron motion. The $\omega_c = qB/m$ is the well known cyclotron frequency of a charged particle (an ion) in a pure magnetic field. If we have an axially harmonic potential in the trap a simple equation relates the cyclotron and magnetron frequencies:

$$\omega_c = \omega_+ + \omega_- \quad (15)$$

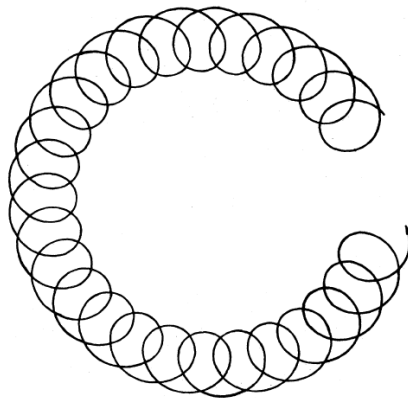


Figure 21: Superposition of the two radial motions in the xy plane of a Penning trap; orbits are not in scale [27].

Fig. 21 visualizes the radial motions in the xy plane (transverse to the magnetic field). Under conditions that are normal for Penning traps (field 1-6T, low voltages on end electrodes) the frequencies of each motion have the following hierarchy $\omega_+ \gg \omega_z \gg \omega_-$. The energy in cyclotron motion is mostly kinetic, for axial motion the energy runs from kinetic to potential as the particle moves in the harmonic potential. If we reduce the energy of these motions their amplitudes are reduced as well, thus these motions are stable. On the other hand as it is pointed out in [27] the magnetron motion is different as it is almost only potential energy. Magnetron motion is a slow motion around the potential hill in the centre of a Penning trap; thus a decrease in energy leads to increase in radius of motion and eventually the particles hit the wall⁶. Fortunately the damping of magnetron motion in Penning traps is slow and the time needed to hit the walls is years. Thus one can assume that if the cyclotron and axial energies are reduced the magnetron motion is untouched and gradually increases its amplitude.

5.3 Sideband cooling

In order to reduce particles' radii in a Penning trap and thus to compress the antiproton cloud in AEGIS; sideband cooling technique can be used. This

⁶As if they would roll down from the potential hill.

method of centering of charged particles is used routinely in Penning traps at experiments with matter such as the ISOLTRAP at CERN ISOLDE facility [26]. In general a buffer gas (or just residual gas) is needed for such compression of plasmas; quite recently this method was also successfully implemented to antiproton cloud centering by using electron cloud instead of buffer gas [25]. The technique is based on a detailed study of classical motion of individual particles in Penning traps (Sec. 5.2).

Sideband cooling allows to dump both of the radial components ω_{\pm} . The central electrode of a Penning trap is divided into four equal segments (radially) and a quadrupole radiofrequency signal is applied to them. The frequency of the the signal is chosen to be the same as the true cyclotron frequency ω_c , then the two radial motions become mixed and their amplitudes are periodically converted from pure magnetron to pure cyclotron motion. Thus if a cooling buffer gas (in case of antiprotons an electron cloud) is introduced along with the radiofrequency signal, the modified ω_{+} frequency is being dumped. But since the Eq. 15 holds this leads to increase in the magnetron frequency and thus the position of an antiproton moves toward the centre. This effect of sideband cooling is shown in Fig. 22. Due to the annihilation of antiprotons, charged particles instead of neutral ones are used for sideband cooling. With that being done additional difficulties are encountered which leave restrictions on the frequencies, electron densities and driving RF voltages, that can be used to efficiently center and cool the antiprotons. Even with the difficulties encountered it was possible to observe sideband cooling at the ATHENA apparatus [25] and it is anticipated to be used in AEGIS as well.

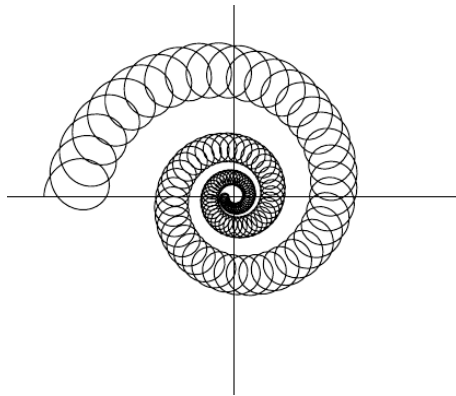


Figure 22: The centering and compression effect of sideband cooling on a charged particle in a Penning trap; a schematic view in the xy plane [25].

5.4 Rotating wall technique

Another way of plasma compression is via rotating electric field. In this case the electrodes of the trap are in Penning-Malmberg configuration (ref Fig. 14). In Penning-type traps a drag on the plasma is created by the natural electric field inhomogeneities and collisions with the background gas. As a result the plasma blows up radially and eventually particles are lost on the electrodes. It was shown [28] that when deliberate rotating electric field asymmetry is introduced

on the central electrode the plasma radius may be increased, kept constant or even be compressed. This effect is attributed to the rotation and changes in the angular momentum of plasma. The plasma $\mathbf{E} \times \mathbf{B}$ rotation frequency f_E is given by

$$f_E(r) = \frac{v_E}{2\pi r}, \quad (16)$$

where v_E is the $\mathbf{E} \times \mathbf{B}$ drift velocity and r is the radial coordinate. A radiofrequency driving signal V_D is put on four (or more) segments of the central electrode of the Penning-Malmberg trap

$$V_D = A_D \cos[m(\phi_i - 2\pi f_D t)], \quad (17)$$

where ϕ_i is the phase on the i -th electrode and f_D is the driving signal frequency. The m component in Eq. 17 is the mode of the electric field; values with $m = 1$ are preferred as they have less significant counteracting harmonics. Depending on the so-called central slip frequency $\Delta f \equiv f_D - f_E(0)$ the rotating wall technique is compressing or blowing up the plasma [28]. For $\Delta f < 0$ the plasma rotation is decreased (rotating field acts as an additional drag) leading to increase in radius. When $\Delta f > 0$ then the plasma rotation frequency increases (plasma being “spinned up”) and consequently the plasma is radially compressed. When the frequencies match and $\Delta f = 0$ it is even possible to maintain the plasma radius constant.

During the rotating electric field application the energy of the plasma is increased and its temperature rises [28]. This is attributed to the change in the density of plasma which changes the on-axis potential and to the excitation of plasma modes due to unwanted $m = 0$ components. In order to compress, cool down and sustain plasmas for a long time some cooling mechanism must be present. In the positron accumulator (Sec. 4.2) cooling of positron plasma is done by collisions with the nitrogen buffer gas. In the antiproton rotating wall compression a cloud of electrons that cools (itself) down by the emission of synchrotron radiation must be present.

The above mentioned methods (sideband and rotating wall) cool down antiprotons using electrons that radiate the excess energy by synchrotron emission. One limit for such cooling is the ambient temperature of the trap since electrons eventually come into an equilibrium with the blackbody radiation. Thus (besides the 100mK region) in most parts of AEGIS 4.2K will be the minimum temperature of the antiproton and electron cloud. So far the Joule heating effect which can substantially increase the temperature of the antiproton cloud was ignored. In Joule heating - due to the above mentioned plasma blow-up in non-ideal traps - the radial increase causes the plasma potential energy decrease, which in turn warms up the plasma. In AEGIS calculations show that Joule heating could be overpowered provided that high quality traps with small electrical inhomogeneities and a good alignment with the magnetic field are constructed. In that case Joule heating could be overpowered by synchrotron or resistive cooling (in the 100mK region) [4].

5.5 Resistive cooling

When going down in ambient temperature below the 4.2K (for eg. in the AEGIS 100mK formation region) the cyclotron motion of electrons becomes

decoupled from the environment due to a small number of blackbody radiation photons with frequencies close to the cyclotron frequency that could be absorbed by the electron. At these temperatures cyclotron motion is governed by the laws of quantum physics. For electron in an ideal Penning trap the potential of the nucleus is replaced by the quadrupole field of the trap, this configuration is called the geonium atom [27]. For such electron the cyclotron motion energy levels are

$$E_c = \hbar\omega_+ \left(n_c + \frac{1}{2} \right) \quad (18)$$

The electrons in cold traps reach the fundamental state with $n_c = 0$ by emission of radiation. Minimum cyclotron energy in the 1T AEGIS formation region is

$$E_{c\min} = (1/2)\hbar\omega_+ \approx \frac{\hbar q B}{2m_e} = 5.79 \times 10^{-5} eV \approx 0.67K \quad (19)$$

Since this cyclotron motion is in the fundamental state the electron cannot give any energy to the antiproton cloud, nor it can receive any energy from antiprotons that are cooler than 0.67K. This is the limit of the synchrotron emission damping of electrons in 1T field⁷.

In order to achieve lower temperatures the antiprotons will be cooled down through the axial motion of the electrons. The radiation rate of the axial motion ω_z is negligible. In order to cool the axial motion so that one can reach the ultimate temperature of 100mK the resistive cooling technique will be used [27].

Resistive cooling relies on the measurement of induced current in an inductor surrounding the Penning trap. As the trapped electrons oscillate along the axis from one endcap to the other they create a RF signal on the endcap electrodes of the trap and induce a current in an RLC circuit surrounding it (the circuit is tuned to the axial frequency ω_z). An idealized scheme of such circuit is shown in Fig. 23. The frequency ω_z is in the radiofrequency range (MHz).

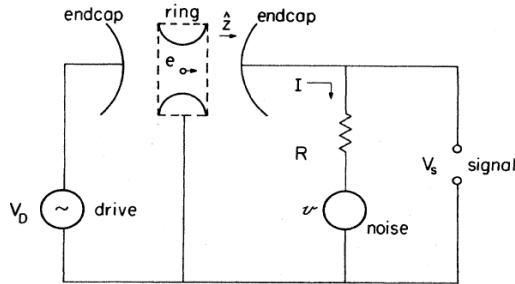


Figure 23: An idealized schematic of the resistive cooling circuit; The tunable driving RF voltage V_D is used to resonantly increase the amplitude of axial oscillation so that ω_z could be distinguished from the noise. [27]

Once the electrons pass the centre of the trap they induce a current i which along with the resistance R of the circuit (R being parasitic from the circuit components) induces a voltage difference iR between the endcap and the ring

⁷In case of higher fields the cooling limit (based on Eq. 19) is even higher.

electrode (Fig. 23). This voltage drop causes electrostatic damping force acting against the movement of the passing electrons. The wires of the RLC circuit will be made out of superconducting material and the whole circuit will be at 100mK. It is expected to cool down the antiproton cloud to 100mK temperature within tens of seconds.

5.6 Antiproton laser cooling via negative ions - the UNIC project

All of the above mentioned cooling methods are limited by the ambient temperature of the trap. To perform high precision gravitational or spectroscopic measurements a lower antihydrogen temperature than 100mK is needed. One method (described in Sec. 8) is to cool the already formed antihydrogen with lasers - this needs trapping of antihydrogen and the use of Lyman- α laser. The other approach is to cool down the antiprotons below the mK range prior to antihydrogen formation. A novel technique of cooling antiprotons through collisions with laser cooled negative ions is currently being investigated at the UNIC project (Ultracold Negative Ions by indirect laser Cooling) at Max Planck Institute in Heidelberg [29] [30]. Even though the cooling technique has not yet been demonstrated, if successful it might have a dramatic impact on the cold antimatter research.

Laser cooling of ions in electromagnetic traps is a regular technique. The principle is based on the fact that ions in a trap are excited by directed photons, but the spontaneous emission in which the ion returns to its ground state is isotropic. The so-called Doppler cooling is done by having laser frequency tuned slightly below the transition frequency (energy) in the ion; only the ions moving fast enough towards the light source are capable of absorbing a photon with the help of Doppler effect. When the ion re-emits a photon it does so isotropically. After many absorptions and emissions the ion cools in the direction of the laser. The photonic field must not be too dense so that stimulated (directed) emission would not dominate over the spontaneous emission. To cool the ions in all directions the Doppler de-tuned laser is directed from all directions or the ions cool in other directions by sympathetic cooling. The limit of laser cooling is the Doppler temperature T_D , which is related to the natural Doppler linewidth of the transition; for Lyman- α laser cooling of (anti)hydrogen this temperature is $T_D = 2.4mK$.

The laser cooling scheme of antiprotons was suggested in [29]. As antiprotons do not have internal structure available for laser excitation other ions might be used to sympathetically cool them down through Coulomb collisions. If regular positive ions would be used, the antiprotons would annihilate quickly as they would be attracted to the positive nucleus. Thus negative ions are the only option for such laser cooling scheme. The Os^- ion is the only known negative ion that has an excited state with a different parity than the ground state and thus the electric-dipole transition is allowed. The bound excited state of Os^- with excitation energy of 1.066eV and a natural linewidth of $\Gamma \approx 10kHz$ has a Doppler temperature $T_D \approx 0.24\mu K$ [29]. If successfully utilized for laser cooling the negative Osmium ion could thus in principle cool down antiprotons to μK range.

6 Positron transfer in AEGIS

In this section the proposed positron transfer line for AEGIS is presented. First the goals to be achieved are presented, then the solutions chosen are outlined. Since in the beginning there were more possible approaches to the problem of injection of positrons and there were not that many restrictions on the specific method of injection, I briefly describe the solutions in a chronological order. In section 6.4 the finalized version of the positron transfer line for AEGIS is presented.

Since the positron bunch would be transferred from the positron accumulator into the main magnet at maximum keV energies a decision to guide the positrons into the apparatus along the magnetic field lines was undertaken. Thus the natural field lines of the main coils were altered in the direction needed for the safe transport. Numerous magnetic field simulations were undertaken in the OPERA 3D simulation software before a decision was undertaken. OPERA 3D is an electromagnetic simulation software distributed by Vector Fields [33], it can solve practically any electro-magnetic problem using the finite element method. In its post-processor OPERA has a particle tracking in-built routine included. When only non-magnetic materials and coils are used the magnetic field at a given point is calculated analytically by solving the Biot-Savart law. This was our case, since we avoided magnetic materials and decided to guide positrons using coils only. It is important to note that the particle tracking was done in a single particle regime. A confirmative calculation taking into account the collective effects of the positron cloud should also be performed in the future. But this would be above the scope of this thesis.

After a series of simulations and decisions on the vacuum components, the diagnostics and the positioning of the positron accumulator the positron transfer line (device) is proposed (Sec. 6.4).

6.1 Requirements on the positron transfer

As mentioned before; in AEGIS the antiprotons from the AD are injected from one side of the superconducting magnets. On the other side of the main magnets there are the Moiré gratings for the gravity measurement. Thus the positrons created in the positron accumulator (4.2) cannot be injected along the main coils' axis as in the case of the ATHENA experiment [5]. There is a need to inject the positrons from an initial position that is off-axis.

Positrons need to be injected into the 5T catching trap (section 4.5) under these requirements:

- Positrons are injected at maximum radius of 1,5cm from the main AEGIS axis.
- After the e^+ cloud compression in the 5T magnet the positrons need to be safely transported to the 1T magnet recombination region.
- Homogeneity of the magnetic field in the 5T and 1T regions needs to be preserved.
- Rapid changes in the magnetic flux in the close vicinity of the cryostat are prohibited due to dilution refrigerator and the induction of eddy currents.

- A minimum magnetic flux of 0.1T should be maintained at all points of the transfer section.
- There has to be space for valves, diagnostics and other vacuum components.

The setup of the main coils allows for three places where external apparatus or particles can be inserted: on both ends or in the central region between the 5T and 1T magnets. On one side there are the already mentioned gratings, thus there are two possibilities for injection of positrons: from the AD side or from the central instrumentation region. If we assume to go from the AD side there are additional requirements that we need to take into account:

- The vacuum of the experiment has to be divided from the AD beam line.
- Degraded used to slow down the 5.3MeV antiprotons has to be removable to allow for positron injection.

6.2 e^+ injection through the central region

The injection from the centre has some principal advantages and disadvantages. In this case the connection between the AD and AEGIS could be done in a similar manner as in the ATHENA experiment [5]. There the first foil of the degrader was a vacuum separation foil made of stainless steel with thickness of $25\mu\text{m}$, followed by the other degrading foils ($130\mu\text{m}$ Al foil and $67\mu\text{m}$ thick Silicon beam counter). On the other hand, when injecting from the centre the space for guiding and correction coils is limited and the magnetic field in this region is high (1-3T) and directed mainly along the main axis.

In Fig. 24 is the picture of one of the first simulations on the possible injection from the middle. There were many difficulties encountered. The main problem in the injection from the centre is that to inject the positrons close to the main axis the transfer coils (perpendicular to the main axis - Fig. 24) have to have a magnetic flux of the same order as the local field. Such coils would have to be superconducting and with a maximum flux of higher than 2T. With the use of opposing balancing coil one could still maintain a high homogeneity region in the 1T main coil. Unfortunately the positrons were injected off-axis at radii above the requirements; in addition the compressed cloud would have been blown up above the requirements when being transferred from the 5T coil back to the 1T coil (as seen in Fig. 24). Also in this setup one would have very limited means to make efficient corrections of the positron trajectories. This approach would also lead to increased complexity of the central instrumentation region which should house not only the dilution refrigerator, but also laser and diagnostics input.

The problems encountered when trying to inject positrons through the central instrumentation region had led to the decision to abandon this possibility and focus on the injection of positrons from the AD side where less problems were initially encountered.

6.3 e^+ injection from the AD side

As explained in the section 6.2 the only place suitable to inject the positrons was found to be between the AD beam line and the AEGIS cryostat. In this case

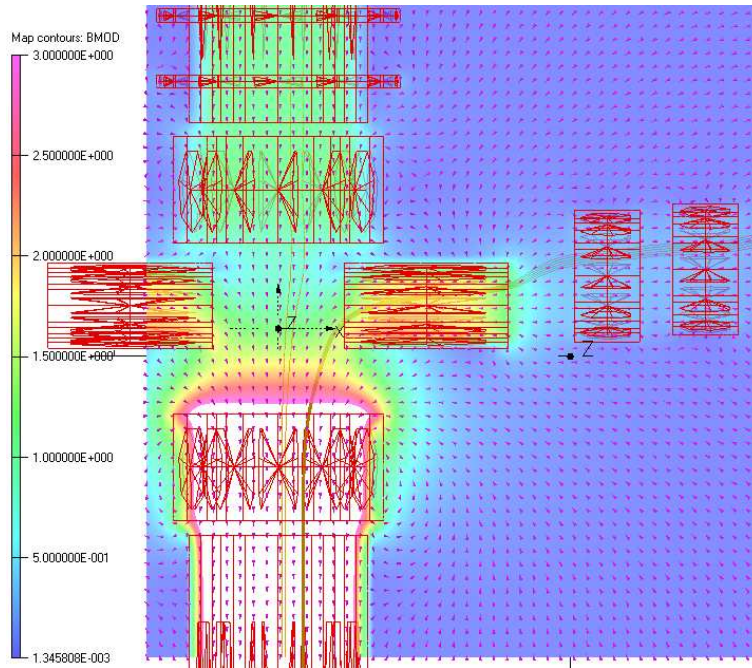


Figure 24: A simulation of injection of positrons through the central region between the 5T and 1T magnets with magnetic field map in [T] and with field direction vectors.

the positron accumulator is located above the AD beam line (figures in section 6.4). The injection from this side avoids most of the problems encountered when transferring the positrons through the central region. If we inject from the AD side:

- The transport of positrons from the 5T magnet to the 1T magnet is undisturbed (is along the axis).
- The field in the central region is axially symmetric.
- The high homogeneity of the main coils is easier to achieve.
- We avoid the use of superconducting transfer coils and the construction of the central part of the cryostat (with the diagnostics and dilution refrigerator) becomes simpler and more economic.

Even though many problems are excluded when injecting from the AD side, one major problem arose. Experiments need to be safely separated from the AD vacuum. This is for two reasons. One, the pressure in AEGIS cryogenic region will be lower than in the antiproton decelerator. The second reason is that in the case of a catastrophic aeration of the AEGIS apparatus the whole AD complex would be aerated as well. To avoid this problem we decided on a use of thin vacuum separation foil that would have long radiation length to allow undegraded passage of antiprotons. Such foil must be as thin as possible and must be able to withstand one sided sudden increase to atmospheric pressures.

Also this foil has to be placed some distance from the AEGIS cryostat (and the degrader) as there has to be space for the positron injection. In this scheme the degrader has to be retractable (in the cryogenic region) from the main axis to allow for the positron injection. A scheme of this concept is in the Figure 25.

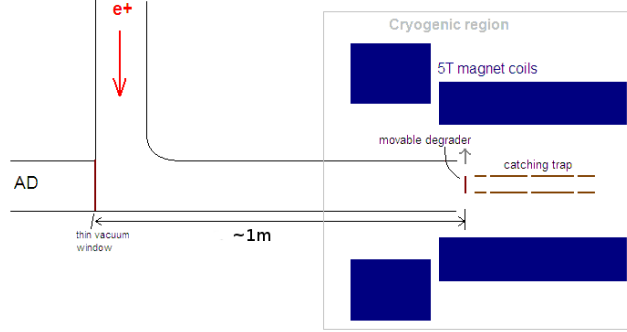


Figure 25: Schematic view of the e^+ injection from the AD side using a retractable degrader and a vacuum separation foil

A Monte Carlo simulation on a number of safe vacuum tight foils was done by A. Fontana⁸ which showed that it might be possible to use this scheme and avoid antiproton losses. The results of vacuum separation foil simulations are shown in Fig. 26. As we can see, the dispersions in energy and angle of the antiprotons

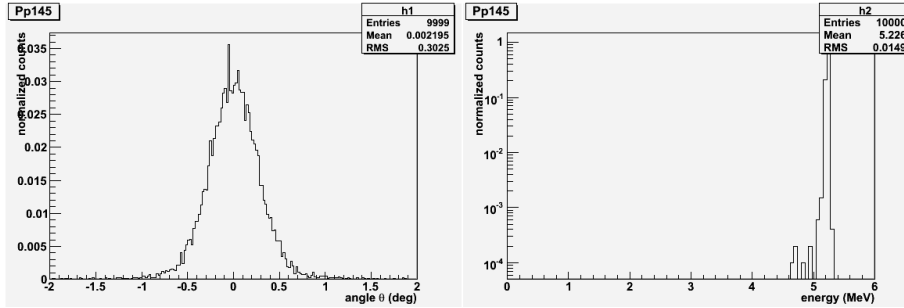


Figure 26: The angular divergence and the energy spread of antiprotons after passage through a vacuum separation foil of $145\mu\text{m}$ thickness.[34]

passing through such foil are relatively low (all the protons fit within 0.9°), on the other hand idealized antiproton beam was used. The $145\mu\text{m}$ thickness seems to be too safe for a vacuum separation foil [32], thus its thickness will probably decrease leading to even lower dispersion. Optimization of this foil is currently under way. As we can see also in the simulations of antiprotons in Fig. 27 even 1° spread in each direction is still within the acceptance of the vacuum chamber; especially if we take the 5T magnetic field focusing effect into account. Fig. 27 shows the simulation of antiprotons with beam diameter 1.2cm and 1° spread with the vacuum separation foil being placed more than 1m from the degrader and catching trap; during the antiproton transfer only the axial

⁸from AEGIS INFN Pavia-Brescia group

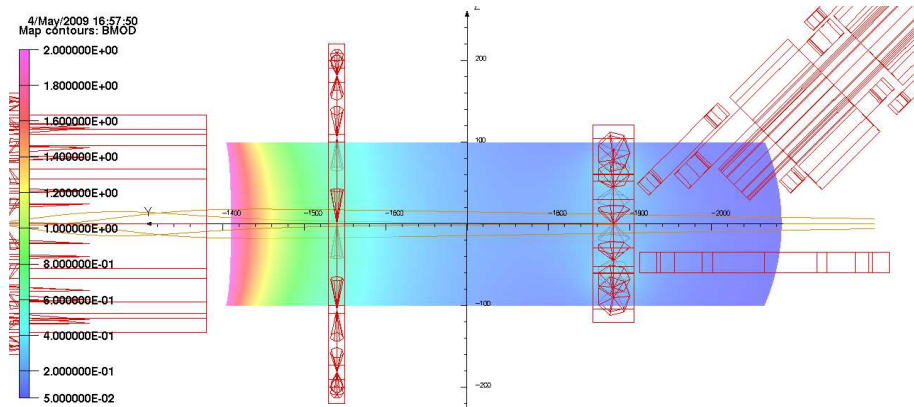


Figure 27: A simulation of 1.2cm antiproton beam with a spread of 1° after passage through the vacuum separation foil - fieldmap on the background (OPERA3D). On the left the 5T magnet, on the right the axial coil of the e^+ transfer line.

coil of the transfer line will be powered. The maximum radial size of antiproton beam is 2cm and thus fits within the DN63 vacuum chamber. Based on the Monte-Carlo (Fig. 26) and antiproton tracking (like in Fig. 27) simulations we decided that the proposed scheme of injection of positrons from the AD side is feasible.

6.4 Positron transfer line proposal

The positron transfer line design presented in this section evolved after series of magnetic field and particle track simulations. The transfer line is proposed using warm copper coils of various geometries without water cooling.

The positron accumulator is located above the antiproton beam line. The positron bunch will be transported into the 5T magnet ballistically; the bunch will be accelerated to 100eV or 1KeV and quickly caught in the 5T catching trap. To transfer the positrons from the positron accumulator to the main magnets' axis solenoids will be used as the main magnetic guides and racetrack coils in a Helmholtz-like geometry will be used for transverse track corrections and additional guidance. These two coils are shown in Figure 28.

Since the positron is a light particle and in our case it has energy in the range from 10 to 1000eV it obeys the magnetic field line at 0.1T (see Tab. 1). The positrons thus are confined radially by the field and they gyrate around the field line and travel in the axial direction. The racetrack Helmholtz coils (Fig. 28) create a dipole field, however there is a stronger (0.1T) field component along the solenoid's axis and thus the dipole component of the Helmholtz coils only changes the overall direction of the 0.1T vector. In this way the particles in the combined fields are bent in the direction of the dipole (Helmholtz) field⁹. A simulation of on axis injection of positrons (with initial radius of 1cm in the positron accumulator) is shown in Fig. 29; even though the positrons travel into

⁹As opposed to regular beam optics case, where the only component present in a dipole magnet is the dipole field, which causes the particles to turn in a direction that is perpendicular to the field vector.

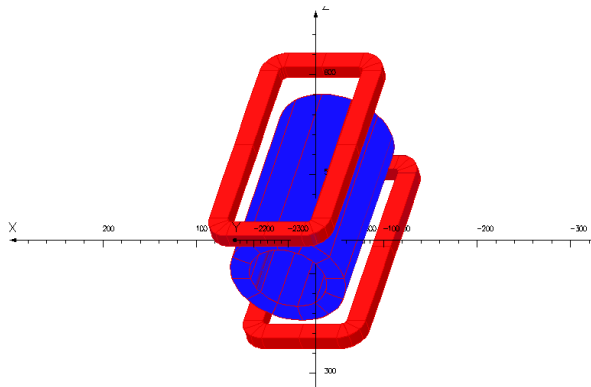


Figure 28: The guiding solenoid (in blue) of the transfer line ($B > 0.1\text{T}$) surrounded by the racetrack helmholtz pair used for effective particle trajectory corrections.

the 5T magnet at one point at large radii ($\approx 1.7\text{cm}$ off-axis) they are compressed in the 5T field into 0.4cm off-axis position.

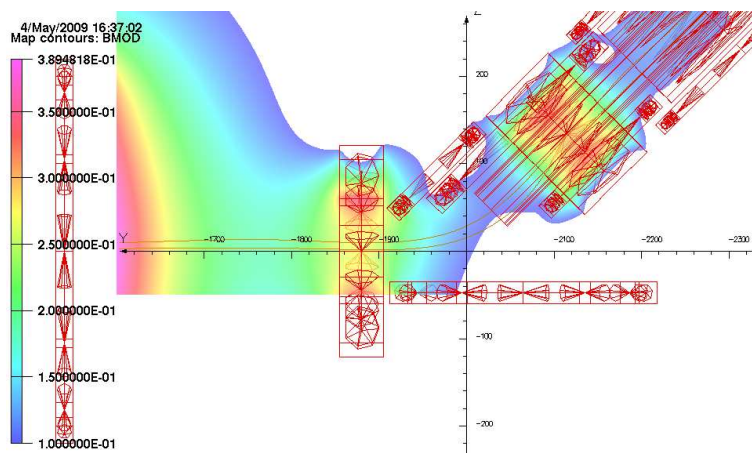


Figure 29: A simulation of on-axis injection of positrons at the AD-AEGIS instrumentation region. On the left the 5T anticon. Horizontal axis aligned with the main AEGIS axis; units in mm; fieldmap limited spatially and by 0.1T value.

A three dimensional view of the coils of the transfer line is shown in Fig. 30, where the racetrack coils are drawn only in one perpendicular direction to the transfer line axis. In real operation we anticipate a possible need for some additional correction racetrack pairs that will be placed in the other transverse direction so that we can correct the paths in all possible directions. A side view of the whole design with each coil marked is shown in Fig. 31. Besides the main 0.1T guides (coils Guide_1-6) and racetrack or solenoid correction coils of various sizes there are also three high power (above 1kW DC) guiding solenoids. These are used to overcome the regions where the coils could not be inserted

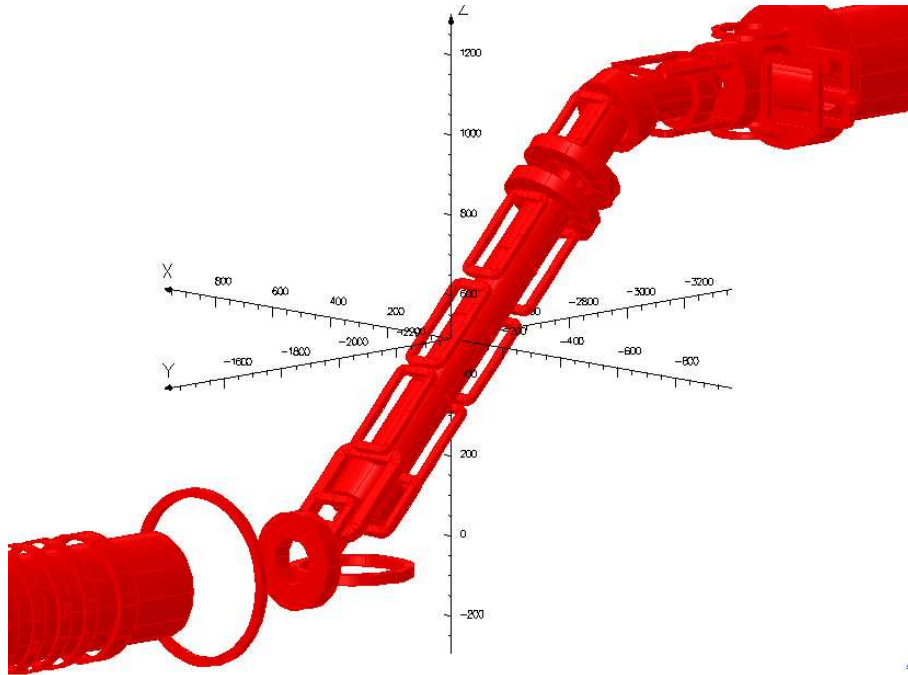


Figure 30: A three dimensional view of the coils of the positron transfer line; in the bottom left corner the 5T magnet, on the top right the positron accumulator.

(two pumping regions and one diagnostics region). The P_Guide_1 coil (Fig. 31) has the power take-off of minimum 1.5kW with on axis magnetic flux of 0.3T. Its geometry is optimized to assure that the field in the positron accumulator pumping and diagnostics area does not drop below 0.1T. The other two coils that each take more than 1kW (the P_Guide_2 and the Axis_coil) are used for the same purpose in the so-called AD-AEGIS instrumentation region, where the main pump for AEGIS will be situated.

The positron transfer line has an additional output in a perpendicular direction at the positron accumulator pumping section (visible at Fig. 30). The extraction of positrons through this output will be done by putting a reverse current in the P_GUIDE_1 coil and by powering the special perpendicular output coil. In this way the positron accumulator can be operated full-time without any dismantling. Thus positrons can be used for improved measurements on positronium formation targets or for other material research.

To limit the gas flow from the positron accumulator into the cryogenic region all the surfaces of the transfer line will be NEG coated; in addition there will be two UHV gate valves along the line, one in front of the positron accumulator and the other valve in front of the cryostat to divide the room temperature region from the cold (4.2K) region. These pneumatically controlled valves will be opened only for the moment when the particle transfer takes place. In addition there will be a pumping restriction (a smaller vacuum chamber) within the high field region of the P_Guide_1 coil to limit the gas flow. The vacuum chamber of the transfer line was optimized to allow for coil insertion and safe positron transport with minimum power input in the coils. The coil support

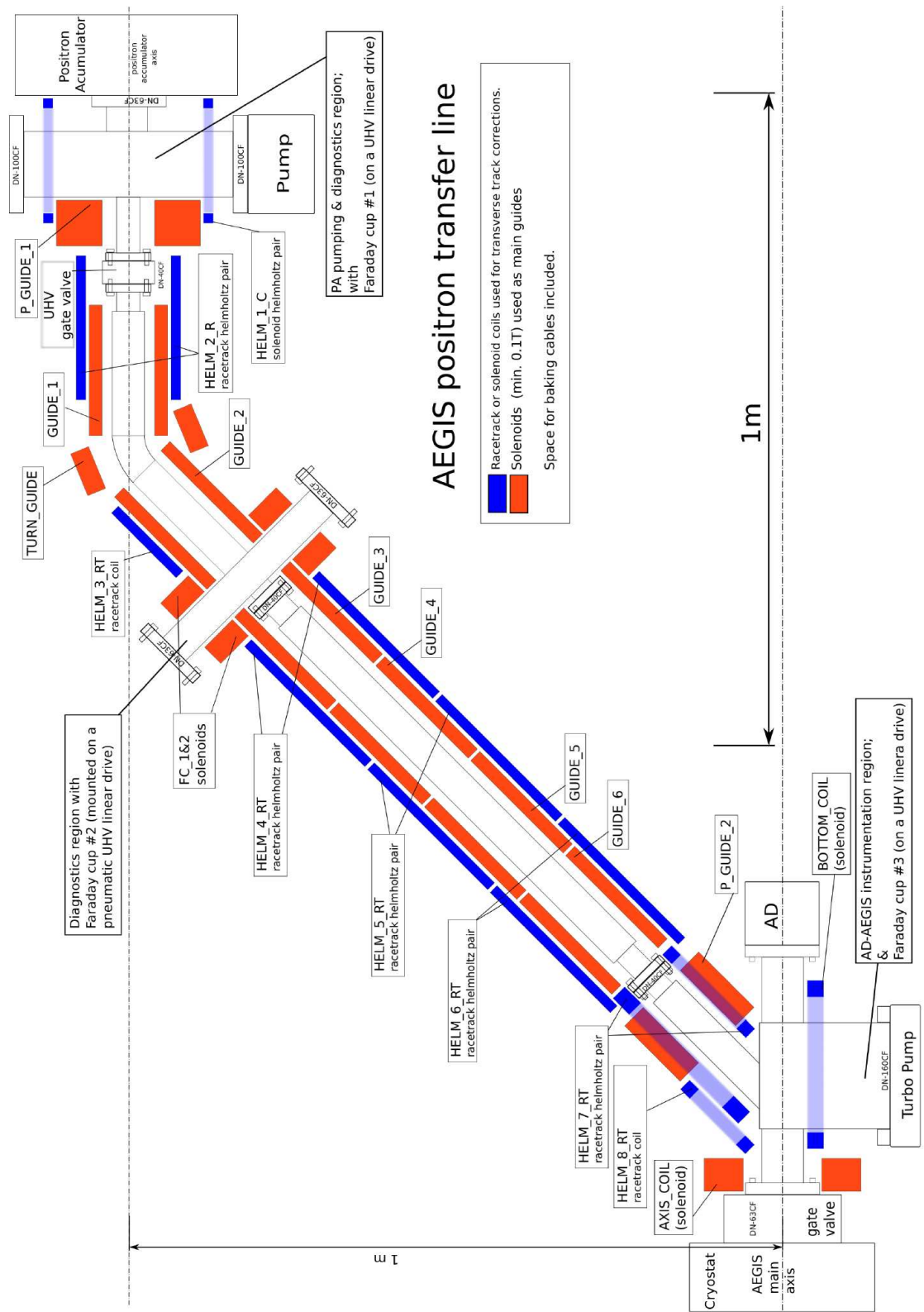


Figure 31: The AEGIS positron transfer (side view) with the vacuum chamber drawn.

materials were chosen to be heat resistant so that the chamber can be baked to high temperatures; if problems are encountered a ventilation space is included between the baking cables and the coil support for active air cooling.

In order to have a good control over the beam during the transfer there are three diagnostics regions with Faraday cup detectors mounted on pneumatic UHV linear drives. One detector (used for the positron accumulation diagnostics) is located at the positron accumulator pumping section. One Faraday cup is mounted in the diagnostics region after the first bend and the last one is in the AD-AEGIS instrumentation region. If additional diagnostics is needed the external scintillation detectors (detecting the 511keV annihilation photons) can also be utilized.

particle	mass [a.m.u.]	$r_{c\ 0.1keV}$ [mm]	$r_{c\ 1keV}$ [mm]
e^+	1/1840	0.3	1.1
p	1	14	46
Ar ⁺	40	91	289
Os ⁺	190	199	630

Table 1: Max cyclotron radii of positron, proton, Argon and Osmium at 0.1T; $r_{c\ 0.1keV}$ and $r_{c\ 1keV}$ are radii at 0.1keV and 1keV energy respectively.

One comment on the use of the positron transfer line for injection of other particles, that are relevant for AEGIS (electrons, protons, Argon ions or Osmium ions). As it was mentioned before the principle of transfer is based on the fact that positrons gyrate around the magnetic field line and that their cyclotron radius is small at the injection energies of 10 - 1000eV. There is no other transverse focusing method applied in the transfer line besides the radial confinement done by the axial field. In table 1 we can see that for light particles (electrons and positrons) at the injection energies the cyclotron radius is small compared to the vacuum chamber dimensions, but looking at the 1840 times heavier proton one can immediately understand that even at very low energies the transfer line cannot be used for other particles than e^+ or e^- . A different injection channel - connected to the AD-AEGIS instrumentation region - will be used for heavier particles.

7 Gravity measurement

In the first phase of AEGIS experiment trapping and cooling of antihydrogen atoms is not envisaged. The temperature of the produced cold antihydrogen will be determined by the temperature of the antiprotons that created it. The antiprotons are expected to be cooled down to 100mK. In Fig. 32 we see an example (a simulation [4]) of antihydrogen velocity distribution after Stark acceleration, where the produced antihydrogen cloud was at 100mK (Maxwell-Boltzmann distributed) with Rydberg states being in Gaussian distribution with $n_{mean} = 30$ and with $\sigma_n = 4$. For interferometric measurements, parameters like the ve-

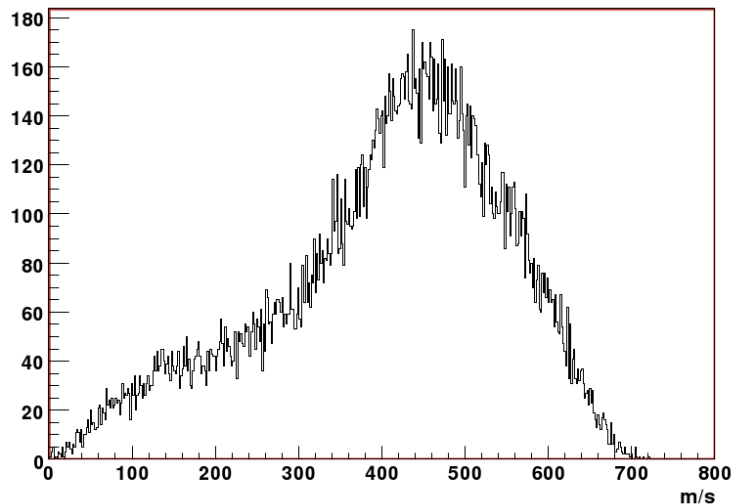


Figure 32: Expected velocity distribution of Stark accelerated 100mK antihydrogen atoms [4].

locity distribution of a beam in Fig. 32 are unacceptable and would ruin the gravity measurement. Since in the first phase of AEGIS no radial cooling of the antihydrogen beam is expected it was chosen to make the first measurement of gravity on antimatter using a classical (without interference) Moiré deflectometer. Moiré deflectometer was used already in gravity measurements on matter by M. Oberthaler et al. [35]. As it will be presented in the latter sections for 1% measurement such a deflectometer does not need a collimated monoenergetic beam coming from a point-like source.

In the consequent sections the basic principles of the Moiré deflectometer measurement will be introduced and also the challenges that need to be met in order to measure the gravitational acceleration with the 1% precision.

7.1 Classical Moiré deflectometer

In the first phase of the experiment the measurement of gravitational acceleration will be done by using the classical Moiré deflectometer. Measurements on Argon gas using the deflectometer have been done with precision below 1% was done by Oberthaler's group. Their setup is shown in Fig. 33. The motion of atom in a Moiré deflectometer is classical, there is no interference occurring.

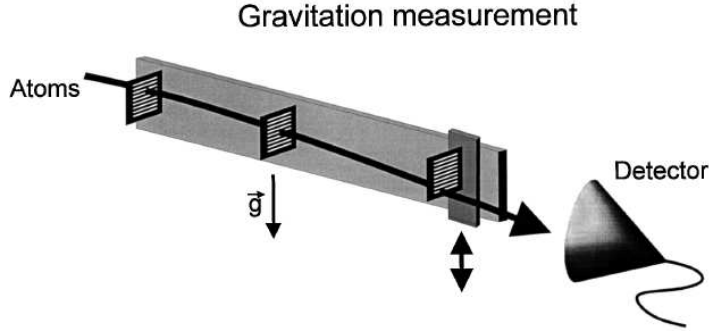


Figure 33: A schematic of the experimental setup used for gravity measurement with Moiré deflectometer. [35]

For interference to occur the wavelength of the phenomena must be similar or greater than the grating period a . If we want to observe interference of matter waves and thus construct an atom interferometer we need a grating period a smaller than the de Broglie wavelength λ_D of atoms:

$$a \ll \sqrt{\lambda_D L} = \sqrt{\frac{hL}{mv}}, \quad (20)$$

where h is the planck constant, m and v is the mass and velocity of the atom and L is the distance between the interferometer gratings. For the deflectometer to work as an (anti)hydrogen interferometer it would have to have grating period $a \ll 13\mu m$ (assuming $v = 1000m/s$, $\lambda_D = 3.96 \times 10^{-10}m$, $L = 0.4m$). In AEGIS $L = 40cm$ and $a = 80\mu m$ grating period is envisaged thus being safely in the classical regime, where interference is negligible. In the Argon experiment by M. Oberthaler et al. a deflectometer with grating period of $13\mu m$ and slit width of $3\mu m$ in each period and with $L = 27cm$ was used.

A classical Moiré deflectometer is well suited for gravity measurement of divergent beams. Basically it is an upgrade to three colimator slits where the first two colimate the divergent beam and the third one is moved up or down to measure the intensity. In the classical (atom) deflectometer we increase the overall transmission (and thus have higher statistics) by putting three gratings at the same distances L from each other. A principle of Moiré deflectometer is shown in Fig. 34.

Behind the third grating there is an integral detector which measures the intensity of the incoming beam. As the third grating is moved vertically we get a modulation of the incoming signal; by knowing the vertical displacement (with superior accuracy compared to a) of the 3rd grating we thus have a position sensitive detector in the vertical direction. And we can measure the shifts in the vertical direction due to the force of gravity.

7.2 AEGIS Moiré deflectometer and the gravity measurement

The schematic of implementation of the Moiré deflectometer in AEGIS is shown in Fig. 35 where the dimensions are not in scale. It is foreseen that in

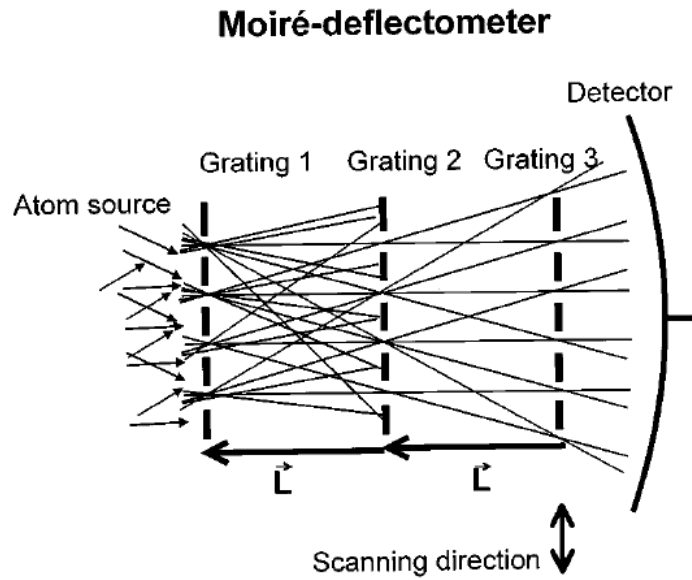


Figure 34: The principle of the classical (Moiré) deflectometer. The diverging atom beam is collimated using two gratings, the third grating is used for detection. [35]

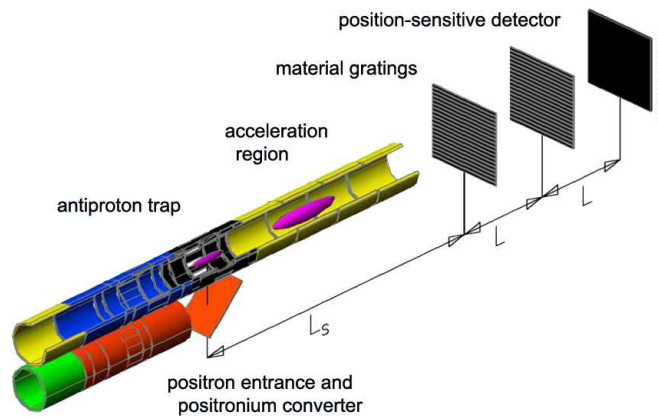


Figure 35: A schematic view of the gravity measurement gratings (Moiré deflectometer) and the antihydrogen formation region (not to scale). [4]

AEGIS the distances between the gratings will be $L = 40\text{cm}$ and the distance from the antihydrogen formation region will be $L_s = 30\text{cm}$. The grating period a will be $80\mu\text{m}$. The main upgrade of the classical deflectometer used in [35] is in the substitution of the third grating by a position sensitive silicon detector and by overall greater dimensions of the gratings (20cm in diameter) due to the relatively large radial velocity (tens m/s without cooling) of the antihydrogen beam. With the position sensitive detector in place no movement is needed as one can record the whole Moiré (fringe) pattern at one moment; also one reduces the need for higher number of antihydrogen measurements and has better statistics. A Silicon strip detector of size $20\times 20\text{cm}$ with a strip pitch of $25\mu\text{m}$ having a resolution below $10\mu\text{m}$ will be used for the g measurement. Additional *Si* strip detector plates are foreseen to be added behind this detector to search for pions coming from the annihilations of antiprotons in the silicon; then the resolution and detection efficiency will increase.

In order to measure the gravity induced vertical displacement on the antihydrogen beam the so-called (gravity induced) phase shift Φ_g is measured. The phase shift Φ_g is the displacement of the beam given in units of the diffraction grating period a (thus being in radians):

$$\Phi_g = \frac{2\pi}{a} g \frac{L^2}{v^2} = \frac{2\pi}{a} g T^2, \quad (21)$$

where g is the gravitational acceleration and v is the velocity and T is the time-of-flight of the antihydrogen between the gratings. The phase shift Φ_g is expressed in radians, because the unit of displacement of the fringe pattern on the detector is measured in relation to the grating period, leading to units y/a (where y is the vertical displacement). The time-of-flight is known from the arrival time of the antihydrogen on the detector and from the end time of Stark acceleration. Even though both of these times are not exact (due to the velocity distribution) it was shown that by careful time-based analysis of the fringe pattern the detected signal can be equivalent to few measurements at different \bar{H} velocities. In this way more phase shifts are measured for one \bar{H} spill.

In Fig. 36 a simulation of the fringe pattern at the position of the third grating is shown, in this case the gravity force is excluded. In Fig. 37 the same simulation and fringe pattern as in Fig. 36 was done, but this time with the gravity vertical shift included in the calculation. In both figures the top plots show a simulation of an extended source with radial velocity $v_r = 0$, the middle plots are showing pattern created by a point-like source with the 100mK M-B velocity distribution used in Fig. 32 and the bottom plots are referring to the most realistic case: an extended source with the 100mK velocity distribution. In both figures it is clear that even with non-ideal divergent beams the phase shift due to gravity using the classical Moiré gratings can be measured. In Fig. 36 the 30% opening in the gratings (which was optimized in [35]) is visible. The presented figures do not take neither the detector efficiency, nor its finite resolution and the gratings imperfections into account. Considering a detector with infinite or finite resolution a more realistic fringes appear (Fig. 38). Since it is not easy to find the exact phase shift Φ_g from Fig. 38 due to lack of statistics in each spill of antihydrogen and due to a spread in velocities, a data analysis procedures are currently studied to obtain the phase shift from Fig. 38. One technique has promising results. It is based on analysis of the flight time of the

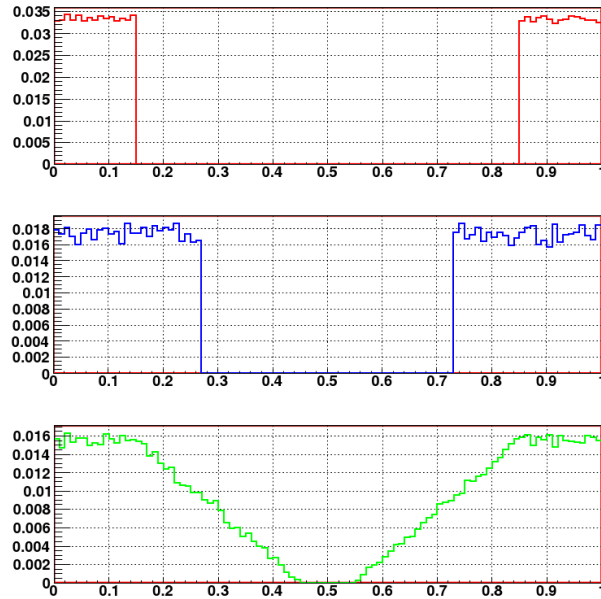


Figure 36: A simulation of number of atoms at the third grating (detector) in AEGIS with respect to y/a . Force of gravity is excluded. Red plot - extended \bar{H} source with $v_r = 0$; blue plot - point-like source with 100mK \bar{H} velocity distribution; Green plot - an extended source with 100mK velocity distribution. [4]

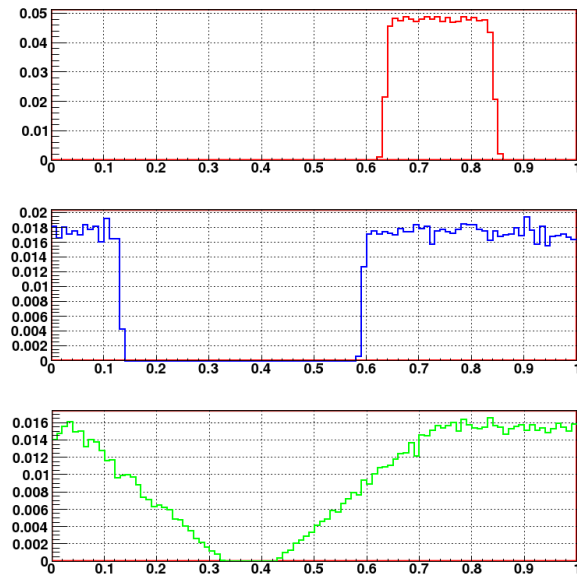


Figure 37: A simulation of number of atoms at the third grating (detector) in AEGIS with respect to y/a . Force of gravity is included. The same nomenclature as in Fig. 36 is used. [4]

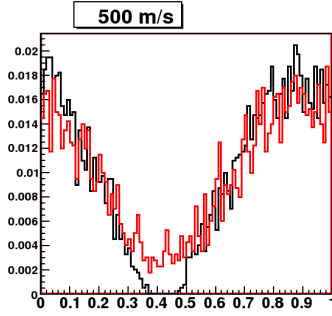


Figure 38: The fringe pattern visible on the detector with finite (red) resolution $\sigma_{det} = 10\mu m$ and infinite (black) position resolution (simulation with 4000 counts). [4]

incoming antihydrogen. If we group the antihydrogen by its time of arrival it is possible to distinguish different phase shifts for each flight-time group. The antihydrogen are grouped based on the time-of-flight squared T^2 distributions.

The measurement of the phase shift would be done by changing the acceleration voltage of antihydrogen resulting in mean velocities from $200m/s$ to $600m/s$. In addition during every measurement (spill of \bar{H}) one can group the detected signal based on the time-of-flight distribution and thus distinguish phase shifts for different velocities in each measurement. Putting all the measured phase shifts ϕ_g and their corresponding time-of-flight T into a graph and interpolating it with Eq. 21 the gravitational acceleration g can be determined. The expected result of the g measurement is shown in Fig. 39.

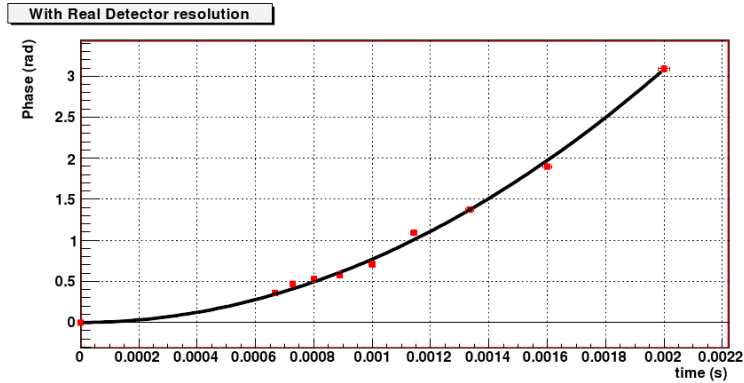


Figure 39: The gravitational phase shift Φ_g as a function of flight time between the gratings T ; a finite $10\mu m$ detector resolution assumed, interpolated via Eq. 21. [4]

Many systematic errors can be encountered during the measurement. To control some of them the gratings will have a possibility to rotate by 90° and thus measure without the effect of gravity. Magnetic field gradients are very dangerous to the measurement since $\frac{dB}{dz} = 10^{-3}T/m$ (for ground state of hydrogen)

gives an equal force to gravity, this means that sufficient magnetic shielding will be surrounding the measurement region [36]. Based on simulations [4] a position sensitive detector with spatial resolution better than $10\mu m$ is needed in order to measure with the 1% precision. Also in order to minimize the errors in the measurement of Φ_g the Moiré gratings and the detector must be vertically well aligned with μm stability; the absolute position (all together) is not influencing the measurement. In order to control the stability of the alignment of the Moiré gratings three laser gratings will be attached to each big grating and the vertical misalignment will be constantly monitored. The horizontal alignment of the gratings is not fatal since it produces blurred images on the detector (reduces the contrast of min and max Fig. 38), but does not cause phase shifts. The distance L between the gratings and between the detector and grating should be the same within two grating periods ($2a$).

8 Beyond the first measurement

As was pointed out in the introduction, AEGIS offers more than just 1% precision measurement of gravitational acceleration. The main goal of the experiment and a large milestone in antimatter physics is the production of cold beam of antihydrogen through Stark acceleration. Once this goal is achieved (thus proving the feasibility of the proposed \bar{H} production techniques) there are many possible upgrades to the apparatus. The first one being the antihydrogen trapping¹⁰.

8.1 Trapping and cooling of antihydrogen

Trapping of atoms can be done in static magnetic traps. Atom traps are routinely used in experiments involving Bose-Einstein Condensates and in other fields [38]. A particle (an atom) with a magnetic moment $\vec{\mu}$ has in a field \vec{B} potential energy

$$V_{\mu} = -\vec{\mu}\vec{B} \quad (22)$$

thus for an antihydrogen in fundamental state with $\mu = 0.67K/T$ a magnetic gradient of $1T/cm$ would confine antihydrogen at $0.67K$ within 1cm. In order to confine hot antihydrogen at 4K the gradients must be comparable to $6T/cm$.

ATRAP and the newer ALPHA experiment [37] (both located at the CERN AD) continue their quest in creating and also trapping the cold antihydrogen atoms in one multipole trap. None have been succesful in this goal so far as it seems that the temperatures of the produced antihydrogen are too high for catching in a multipole trap. Even though some positive results have been shown, when imersing a Penning-Malmberg trap into sextupole field in the transverse plane [39] it is still not sure if the approach of combining a multipole and Penning-type trap could allow for production and trapping of cold antihydrogen. Storage times in these combined traps are dramatically shorter than in Penning traps with highly homogeneous axial fields. If the prepared cold cloud of antiprotons would be transported into this combined trap only for the moment of \bar{H} production it would still probably heat up during the transfer; in addition the expansion in the combined trap would cause Joule heating of the antiproton (and positron) plasma. While the results on trapping of cold antihydrogen at ATRAP and ALPHA collaborations is eagerly awaited, AEGIS production scheme offers an alternative to the combined traps.

In AEGIS the produced antihydrogen beam can be directed (through Stark acceleration) into a region with different magnetic field, where the trapping can take place. In this way both the produciton and the trapping procedures can be optimized. Such magnetic atom trap would be located at the exit of the 1T magnet, in the gravity measurement region (which will be removed). To trap the antihydrogen it has to lose some energy as it travels inside the magnetic trapping potential. Stark deceleration could be the applied mechanism, that could slow down the antihydrogen in the magnetic trap, so that it could not

¹⁰All of the upgrades at one point or another assume to use Lyman- α laser to stimulate $1s \rightarrow 2s$ or $1s \rightarrow 2p$ transitions in antihydrogen atoms. For an efficient radial cooling of antihydrogen beam such laser would have to deliver 100mW power in approximately $100\mu s$. Currently such lasers operate at CW mode, but with powers in the nW range. Experimental effort by members of AEGIS is under way to produce a quasi-CW Lyman- α laser source for antihydrogen cooling and spectroscopy.

escape the potential well in Eq. 22. The antihydrogen has to be re-excited into a Rydberg state so that Stark deceleration can take place. This method also needs to be verified in the presence of magnetic field gradients, that could hamper the Stark deceleration techniques.

8.2 Improved gravity measurement using atom interferometry

Once the trapping scheme proves to be successful, many experimental possibilities open up for AEGIS apparatus, one of them being an improved gravity measurement with a use of an atomic interferometer. There have been extremely accurate measurements on the earth gravitational acceleration g for Cesium atoms with sensitivity $10^{-10}g$. Unfortunately there is a need to have a collimated ultracold μK beam of atoms to perform these precise measurements. Such measurement would become feasible with antihydrogen only if the antiproton cooling technique via negative Osmium could be applied or if some other mechanism that cools antimatter to μK range would be developed. On the other hand with Lyman- α laser cooling to couple mK in a magnetic trap it should be possible to perform gravity measurement with 10^{-4} precision in atomic interferometers.

8.3 Antihydrogen spectroscopy and CPT invariance

S in AEGIS stands for spectroscopy and it is a long term goal of the experiment. Having a trapped antihydrogen and a Lyman- α laser it might be possible to do spectroscopic measurement on the $1s \rightarrow 2p$ transition of antihydrogen. Spectroscopic measurements on antihydrogen could give a very precise (10^{-15} and maybe better) tests of the CPT invariance by direct comparison of atomic hydrogen with antihydrogen [4]. Even though the most precise test of CPT is from the K^0 and \bar{K}^0 mass difference (being $|(m_{\bar{K}^0} - m_{K^0})/m_{K^0}| \leq 0.8 \times 10^{-18}$) [40], spectroscopic measurements on antihydrogen would be the most precise test of CPT on baryons.

9 Conclusion

The AEGIS experiment which is currently under preparation will be the first experiment to measure gravitational acceleration on antihydrogen; thus it will also test the validity of the weak equivalence principle on antimatter and test some quantum theories of gravity.

The experiment consists of many components that were described in this work. Antiproton cooling techniques, that are crucial for the antihydrogen production were also described. Novel technique in antimatter research - Stark acceleration - will be used in AEGIS in order to create an antihydrogen (neutral) beam and the gravity measurement will be done using a classical Moiré deflectometer.

The objective of this work was the development of positron transport and injection for the AEGIS experiment. A number of simulations in OPERA 3D software were done in preparation of the positron injection. The positron transfer line, the result of this work, was described in section 6 (shown in Fig. 30 and Fig. 31). The requirements were fulfilled since positrons can be injected using warm coils only onto the main AEGIS axis. A new method of vacuum separation from the antiproton decelerator was successfully implemented in order to inject positrons without significant antiproton losses. The design of the positron transfer line, including the vacuum chamber, was accepted by the AEGIS collaboration.

References

- [1] *AEGIS official webpage*. <http://cern.ch/aegis>
- [2] T. Goldman et al., *Experimental Evidence for Quantum Gravity?*. Phys. Lett. B **171**, 217 (1986)
- [3] T.W. Darling et al., *The fall of charged particles under gravity: A study of experimental problems*. Rev. Mod. Phys. **64**, 1 (1992)
- [4] M. Amoretti et al., *Proposal for the AEGIS experiment at the CERN Antiproton Decelerator* (2007)
<http://doc.cern.ch/archive/electronic/cern/preprints/spsc/public/spsc-2007-017.pdf>
- [5] M. Amoretti et al., *The ATHENA antihydrogen apparatus*. Nucl. Instr. and Meth. A **518**, p679 (2004)
- [6] M. Amoretti et al., *Production and detection of cold antihydrogen atoms*. Nature **419**, 456 (2002)
- [7] G. Gabrielse et al., *Driven Production of Cold Antihydrogen and the First Measured Distribution of Antihydrogen States*. Phys. Rev. Lett. **89**, 213401 (2002)
- [8] C.H. Storry et al., *First Laser-Controlled Antihydrogen Production*. Phys. Rev. Lett. **93**, 263401 (2004)
- [9] D.W. Gidley et al., *Positron Annihilation as a Method to Characterize Porous Materials*. Annu. Rev. Mater. Res. **36**, 49 (2006)
- [10] S.R. Procter et al., *Controlling the motion of hydrogen molecules*. Chem. Phys. Lett. **374**, 667 (2003)
- [11] E. Vliegen, F. Merkt, *Stark deceleration of hydrogen atoms*. J. Phys. B: At. Mol. Opt. Phys. **39**, L241 (2005)
- [12] E. Vliegen et al., *Stark deceleration and trapping of hydrogen Rydberg atoms*. Phys. Rev. A **76**, 023405 (2007)
- [13] J. Main et al., *Hydrogen atom in combined electric and magnetic fields with arbitrary mutual orientations*. Phys. Rev. A **57**, 1149 (1998)
- [14] *Introduction to the AD*.
<http://psdoc.web.cern.ch/PSdoc/acc/ad/MainPage/main.html>
- [15] T.L. Watson, *Accumulation and Manipulation of Positron Plasmas for Antihydrogen Production*, University of Wales Swansea, (2003)
- [16] *SMC Polarized target at CERN*,
<http://na47sun05.cern.ch/target/outline/dilref.html>
- [17] *University of Lancaster Ultra Low Temperature Group*,
<http://www.lancs.ac.uk/depts/physics/research/condmatt/ult/dilut.htm>
- [18] <http://www.phys.washington.edu/users/vilches/LOWTEMP/dilref.html>

- [19] X.Huang et al., *Steady-State Confinement of Non-neutral Plasmas by Rotating Electric Fields*. Phys. Rev. Lett. **78**, 875 (1997)
- [20] J.R. Danielson et al., *Plasma manipulation techniques for positron storage in a multicell trap*. Physics of Plasmas **13**, 123502 (2006)
- [21] R.C. Davidson, *The Physics of Nonneutral Plasmas*. Addison Wesley, Reading (1990)
- [22] G. Testera, *Private communication*
- [23] B. Seligmann, *An Introduction to Electron Cooling*. CAS: 4th General Accelerator Physics Course proceedings, (1990)
Available at <http://doc.cern.ch/yellowrep/1991/91-04/p175.tif>
- [24] L. Spitzer jr., *Physics of Fully Ionized Gases*. Interscience Publishers, New York (1956)
- [25] A. Kellerbauer et al., *Sideband cooling of ions in a non-neutral buffer gas*. Phys. Rev. A **73**, 062508 (2006)
- [26] G. Bollen et al., *ISOLTRAP: A Tandem Penning Trap System for Accurate On-line Mass Determination of Short-lived Isotopes*. Nucl. Instr. and Meth. Phys. Res. A **368**, 675 (1996)
- [27] L.S. Brown, G. Gabrielse, *Geonium theory: Physics of a single electron or ion in a Penning trap*. Rev. Mod. Phys. **58**, 233 (1986)
- [28] X.-P. Huang et al., *Steady-State Confinement of Non-neutral plasmas by Rotating Electric Fields*. Phys. Rev. Lett. **78**, 875 (1997)
- [29] A. Kellerbauer, J. Walz, *A novel cooling scheme for antiprotons*. New. J. Phys. **8**, 45 (2006)
- [30] U. Warring et al., *High-Resolution Laser Spectroscopy on the Negative Osmium Ion*. Phys. Rev. Lett. **102**, 043001 (2009)
- [31] S. Haroche, *Cooling and Trapping Atoms with Light*. (Lecture) Available at [http://ultracold.uchicago.edu/haroche/Phys154Lecture_8\(Serge\).pdf](http://ultracold.uchicago.edu/haroche/Phys154Lecture_8(Serge).pdf)
- [32] T. Niinikoski, *Private communication*
- [33] <http://www.vectorfields.com/>
- [34] A. Fontana, *Private communication*
- [35] M. Oberthaler et al., *Inertial sensing with classical atomic beams*. Phys. Rev. A **54**, 4 (1996)
- [36] M. Doser, *AEGIS: a new experiment to measure the gravitational interaction of antihydrogen*, a talk presented at SMI Seminar zu aktuellen Themen der subatomaren Physik, Vienna (2008)
- [37] *ALPHA experiment official webpage*. <http://cern.ch/alpha>
- [38] *Research groups working with atom traps*. <http://www.uibk.ac.at/exphys/ultracold/atomtraps.html>

- [39] M. Amoretti et al., *Storage of an electron plasma in a sextupole radial antihydrogen trap*. Phys. Lett. A **360**, 141 (2006)
- [40] C. Amsler et al. (Particle Data Group), PL **B667**, 1 (2008)
<http://pdg.lbl.gov>